Asteroid clusters similar to asteroid pairs

P. Pravec [a], P. Fatka [a,b], D. Vokrouhlický [b], D. J. Scheeres [c], P. Kušnirák [a], K. Hornoch [a], A. Galád [a,d], J. Vraštil [a,b], D. P. Pray [e], Yu. N. Krugly [f], N. M. Gaftonyuk [g], R. Ya. Inasaridze [h], V. R. Ayvazian [h], O. I. Kvaratskhelia [h], V. T. Zhuzhunadze [h], M. Husárik [i], W. R. Cooney [j], J. Gross [j], D. Terrell [j,k], J. Világi [d], L. Kornoš [d], Š. Gajdoš [d], O. Burkhonov [ℓ], Sh. A. Ehgamberdiev [ℓ], Z. Donchev [m], G. Borisov [m], T. Bonev [m], V. V. Rumyantsev [n], I. E. Molotov [o]

[a] *Astronomical Institute, Academy of Sciences of the Czech Republic, Fričova 1, CZ-25165 Ondřejov, Czech Republic*

[b] *Institute of Astronomy, Charles University, Prague, V Holešovičkách 2, CZ-18000 Prague 8, Czech Republic*

[c] *Department of Aerospace Engineering Sciences, The University of Colorado at Boulder, Boulder, CO, USA*

[d] *Modra Observatory, Department of Astronomy, Physics of the Earth, and Meteorology, FMPI UK, Bratislava SK-84248, Slovakia*

[e] *Sugarloaf Mountain Observatory, South Deerfield, MA, USA*

[f] *Institute of Astronomy of Kharkiv National University, Sumska Str. 35, Kharkiv 61022, Ukraine*

[g] *Crimean Astrophysical Observatory, Department of Radioastronomy and Geodynamics, Simeiz, 298680, Crimea*

[h] *Kharadze Abastumani Astrophysical Observatory, Ilia State University, G. Tsereteli str. 3, 0162 Tbilisi, Georgia*

[i] *Astronomical Institute of the Slovak Academy of Sciences, SK-05960 Tatranská Lomnica, Slovakia*

[j] *Sonoita Research Observatory, 77 Paint Trail, Sonoita, AZ 85637, USA*

[k] *Deptartment of Space Studies, Southwest Research Institute, Boulder, CO 80302, USA*

[ℓ] *Ulugh Beg Astronomical Institute, Astronomicheskaya Street 33, 100052 Tashkent, Uzbekistan*

[m] *Institute of Astronomy and NAO, Bulgarian Academy of Sciences, 72, Tsarigradsko Chaussee Blvd., 1784 Sofia, Bulgaria*

[n] *Crimean Astrophysical Observatory, RAS, 298409 Nauchny, Crimea*

[o] *Keldysh Institute of Applied Mathematics, RAS, Miusskaya sq. 4, 125047 Moscow, Russia*

2017 June, revised submitted version

Proposed running head: Asteroid clusters

Editorial correspondence to:
Dr. Petr Pravec
Astronomical Institute AS CR
Fričova 1
Ondřejov
CZ-25165
Czech Republic
Phone: 00420-323-620352
Fax: 00420-323-620263
E-mail address: petr.pravec@asu.cas.cz

Abstract

We studied the membership, size ratio and rotational properties of 13 asteroid clusters consisting of between 3 and 19 known members that are on similar heliocentric orbits. By backward integrations of their orbits, we confirmed their cluster membership and estimated times elapsed since separation of the secondaries (the smaller cluster members) from the primary (i.e., cluster age) that are between 10^5 and a few 10^6 years. We ran photometric observations for all the cluster primaries and a sample of secondaries and we derived their accurate absolute magnitudes and rotation periods. We found that 11 of the 13 clusters follow the same trend of primary rotation period vs mass ratio as asteroid pairs that was revealed by Pravec et al. (Pravec, P., et al. [2010]. Nature 266, 1085–1088). We generalized the model of the post-fission system for asteroid pairs by Pravec et al. (2010) to a system of N components formed by rotational fission and we found excellent agreement between the data for the 11 asteroid clusters and the prediction from the theory of their formation by rotational fission. The two exceptions are the high-mass ratio ($q > 0.7$) clusters of (18777) Hobson and (22280) Mandragora for which a different formation mechanism is needed. Two candidate mechanisms for formation of more than one secondary by rotational fission were published: the secondary fission process proposed by Jacobson and Scheeres [Jacobson, S. A., Scheeres, D. J. [2011]. Icarus 214, 161–178] and a cratering collision event onto a nearly critically rotating primary proposed by Vokrouhlický et al. [Vokrouhlický, D., et al. [2017]. Astron. Astrophys. 598, A91]. It will have to be revealed from future studies which of the clusters were formed by one or the other process. To that point, we found certain further interesting properties and features of the asteroid clusters that place constraints on the theories of their formation, among them the most intriguing being the possibility of a cascade disruption for some of the clusters.

Key words: Asteroids, dynamics; Asteroids, rotation; Photometry

1 Introduction

There exist very young clusters (also called mini-families) of asteroids, consisting of a few or several members that separated on an order of 10^5 to 10^6 yr ago. The first four such clusters were found by Nesvorný et al. (2006) and Nesvorný and Vokrouhlický (2006), with the primary [1] bodies (1270) Datura, (14627) Emilkowalski, (16598) Brugmansia = 1992 YC2 and (21509) Lucascavin. Pravec and Vokrouhlický (2009) found five more clusters, with the primaries (6825) Irvine, (10321) Rampo, (18777) Hobson, [2] (39991) Iochroma and (81337) 2000 GP36; the last one was found to be a part of the larger cluster of (2384) Schulhof by Vokrouhlický and Nesvorný (2011). Novaković et al. (2014) found a cluster of (20674) 1999 VT1, which contains also the active asteroid P/2012 F5 (Gibbs). [3] Recently the clusters of (1270) Datura and (2384) Schulhof were studied in detail by Vokrouhlický et al. (2016, 2017). They updated their age estimates and obtained interesting results on their spin, shape and angular momentum properties. In these recent as well as the previous works, the authors generally assumed that the young asteroid clusters, like big and old families in the main belt, were formed by collisions. For the Datura cluster Vokrouhlický et al. (2017) suggested that the swarm of small fragments could be due to a cratering event, rather than a catastrophic disruption, from impact of a small projectile onto the nearly critically rotating primary.

In this paper we study angular momentum and size distribution properties of 13 clusters (including 3 new ones). We will show that the properties of most of the clusters are consistent with an alternative model that they formed by rotational fission of critically spinning parent bodies. Thus, the small and young asteroid clusters resemble asteroid pairs, just consisting of more than one escaped secondary.

2 Cluster membership and age estimation

We study 10 clusters found previously and we include 3 new clusters, with the primary bodies (11842) Kap'bos, (22280) Mandragora and (66583) Nicandra. We found the new clusters as a by-product of our search for asteroid pairs in

[1] The term "primary" is used for the largest body of a cluster. The term "secondary" is used for any smaller member of given cluster.

[2] Pravec and Vokrouhlický (2009) did not reveal it uniquely whether (18777) Hobson belonged to the cluster, they had an ambiguity in identification of the cluster's primary. Rosaev and Plávalová (2017) confirmed that (18777) Hobson belongs to the cluster. We further confirmed it with our backward orbital integrations, see Section 2.8.

[3] Nesvorný et al. (2008) found that the semi-young family around (656) Beagle with an estimated age of several Myr contains (7968) Elst-Pizzaro that is the archetype of active asteroids. These cases suggest that a relation between active asteroids and (relatively) young families is common.

the space of mean orbital elements using the method of Pravec and Vokrouhlický (2009). [4] In each of the three cases, the two closest members of a cluster popped up as seemingly a statistically significant pair, with other candidate members found nearby within the distance limit given below. [5, 6, 7]

The membership of the Datura and Schulhof clusters were analysed in Vokrouhlický et al. (2016, 2017). For the other 11 clusters, we identified candidate members by analyzing distribution of their distances in the five-dimensional space of mean orbital elements $(a, e, i, \varpi, \Omega)$. Analogously to Pravec and Vokrouhlický (2009), the distance ($d_{\rm mean}$) between two asteroid orbits was computed with a positive-definite quadratic form

$$\left(\frac{d_{\rm mean}}{na}\right)^2 = k_a \left(\frac{\delta a}{a}\right)^2 + k_e(\delta e)^2 + k_i(\delta \sin i)^2 + k_\Omega(\delta\Omega)^2 + k_\varpi(\delta\varpi)^2 \,, \quad (1)$$

where n and a are the mean motion and semimajor axis of either of the two asteroids and $(\delta a, \delta e, \delta \sin i, \delta\varpi, \delta\Omega)$ is the separation vector of their mean orbital elements. Following Zappalà et al. (1990) and Pravec and Vokrouhlický (2009), we used $k_a = 5/4$, $k_e = k_i = 2$ and $k_\varpi = k_\Omega = 10^{-4}$. The distance $d_{\rm mean}$ between two asteroid orbits is an approximate gauge for the relative velocity of the asteroids at close encounter (see Rożek et al. 2011 for explicit tests). For asteroid pairs, it is in the range of a few to several tens m/s. To do not miss possible more distant members, we searched for candidate members of each cluster up to $d_{\rm mean} = 100$ m/s from the cluster's primary.

To confirm the cluster membership suggested by the asteroid distances in the space of mean orbital elements, we integrated a set of geometric clones (500 clones for each asteroid) with the Yarkovsky effect acting on each clone differently. The Yarkovsky effect was represented using a fake transverse ac-

[4] Pravec and Vokrouhlický (2009) originally used osculating orbital elements, but later we amended the method with the use of mean elements, following suggestion by D. Nesvorný (2010, personal communication; see also Rożek et al. 2011). The mean elements were taken from the AstDyS catalog webpage (update August 2016; Knežević et al. 2002, Knežević and Milani 2003).

[5] The statistical significance of all the clusters is high. Even for the cluster of Nicandra with the 3 multiple-opposition members at relatively large distances in the space of mean orbital elements, the probability that it could be just a random orbital coincidence of 3 genetically unrelated asteroids is 0.0013 (calculated with the method by Pravec and Vokrouhlický 2009 extended to asteroid triples), and the statistical significance is further strengthened by the presence of two close one-opposition asteroids, see Section 2.13. The probability of random orbital coincidence is lower by many orders of magnitude for all the other, more numerous and/or tighter clusters.

[6] In the case of cluster (11842), the two asteroids (11842) Kap'bos and (228747) 2002 VH3 were found as an apparent pair by Pravec and Vokrouhlický (2009). We revealed that it is actually a cluster after the third member (436415) 2011 AW46 was discovered two years later. See Section 2.5.

[7] As a by-product of the search for asteroid pairs, we also recovered inner cores of the larger and somewhat older collisional families of (832) Karin and (3152) Jones that were discovered by Nesvorný et al. (2002, 2015).

celeration acting on the clone with a magnitude providing secular change in semimajor axis $\dot{a}_{\rm Yark}$ (see Farnocchia et al. 2013). It was chosen from the range $\langle -\dot{a}_{\rm max}, \dot{a}_{\rm max} \rangle$, where $\dot{a}_{\rm max}$ was estimated from the asteroid size (see Vokrouhlický 1999). These minimum and maximum values of the semimajor axis drift rate correspond to bodies with (i) 180° and 0° obliquities, for which the diurnal variant of the effect is optimized, and (ii) diurnal thermal parameter equal square root of two, for which the magnitude of the Yarkovsky effect is the largest (see, e.g., Vokrouhlický 1999). The goal of our backward orbital integrations was to find when clones of the secondary components were close and at low relative velocities to clones of the primary component of a cluster. This corresponds to the situation when the secondaries separated from the primary. In order to express the orbital proximity quantitatively, we chose following limits on the physical distance and relative velocity between the clones $r_{\rm rel} \leq 10-20 R_{\rm Hill}$ and $v_{\rm rel} \leq 2-4 v_{\rm esc}$, where $R_{\rm Hill}$ and $v_{\rm esc}$ are the radius of the Hill sphere and the surface escape velocity, respectively, of the primary body. The narrower limits were used for tighter (typically the youngest) clusters, while for most clusters we used the loosened limits.[8] The radius of the Hill sphere was estimated as $R_{\rm Hill} \sim a D_1 \frac{1}{2} \left(\frac{4\pi}{9} \frac{G\rho_1}{\mu} \right)^{1/3}$, where a is the heliocentric semi-major axis, D_1 is the estimated diameter of the primary body, G is the gravitational constant, ρ_1 is the primary's bulk density (assumed 2 g/cm^3) and μ is the gravitational parameter of the Sun. The escape velocity was estimated as $v_{\rm esc} \sim D_1 \frac{1}{2} \left(\frac{8\pi}{3} G\rho_1 \right)^{1/2}$ (both formulas from Pravec et al. 2010, Supplementary Information).

To further confirm the cluster membership, we also applied the method based on convergence of the secular angles Ω and ϖ by Nesvorný and Vokrouhlický (2006) to 8 of the 13 clusters for which this was not done (or publihed) before. The method attempts to find a convergence in the secular angles for all cluster members at the same time. To find the greatest similarity of Ω and ϖ for all the members, we searched for the minimum of function

$$\Delta V\,(t) = na\sqrt{k_1 \left(\sin i \Delta\Omega\right)^2 + k_2 \left(e\Delta\varpi\right)^2}, \qquad (2)$$

where $k_1 = 1$ and $k_2 = 1/2$ (for discussion of the choice see Nesvorný and Vokrouhlický 2006) and $\Delta\Omega$ and $\Delta\varpi$ represent a dispersion of the angles at time t. The dispersion $\Delta\Omega$ is defined as $(\Delta\Omega)^2 = \sum_{ij} \left(\Delta\Omega_{ij}\right)^2 / [N(N-1)/2]$, where $\Delta\Omega_{ij}$ are the differences between Ω for the i-th and the j-th orbit and N is the number of members in the cluster. The dispersion $\Delta\varpi$ is defined analogously. As this method does not take into account relative positions of the asteroids, to filter most trustworthy convergences, we employed a limit on the dispersion in mean anomaly $|\Delta M| < 90°$ for the clusters of Kap'bos and Nicandra that is defined analogously to $\Delta\Omega$. We note that this method

[8] The relaxed constraints used for members in more dispersed and older clusters reflect our inability to propagate the asteroid orbits with an exact determinism. The smaller accuracy is amplified especially for situations where weak mean motion resonances cross the cluster location or stochastic encounters to massive bodies in the main belt (the dwarf planet Ceres or the largest asteroids Vesta, Pallas or Juno) are most likely.

assumes that all cluster members separated at a single time. This may produce mis-leading results in cases where there were multiple secondary escape events (see subsections on individual clusters below for a few such suspect cases), thus outcomes of this method must be taken cautiously with the given limitation in mind. The results obtained with this method are presented in Electronic Supplementary Information.

For numerical integration we used the Regularized Mixed Variable Symplectic method (RMVS3) developed by Levison and Duncan (1994) from the `swift`[9] package, which was modified to include the Yarkovsky effect (Nesvorný and Vokrouhlický 2006). We included gravitational attraction of the 8 major planets. The geometric clones were created in the six-dimensional space of equinoctical elements $\mathbf{E}$ using the probability distribution $p(\mathbf{E}) \propto \exp\left(-\frac{1}{2}\Delta\mathbf{E}\cdot\Sigma\cdot\Delta\mathbf{E}\right)$, where $\Delta\mathbf{E} = \mathbf{E} - \mathbf{E}^\star$ is the difference with respect to the best-fit orbital values $\mathbf{E}^\star$ and Σ is the normal matrix of the orbital solution downloaded from `AstDyS` website at the initial epoch MJD 57600 (Milani and Groncchi 2010). Each geometrical clone was given a random value of $\dot{a}_{\rm Yark}$ in the range $-\dot{a}_{\rm max} \leq \dot{a}_{\rm Yark} \leq \dot{a}_{\rm max}$.

For each secondary, we estimated a time since its separation from the primary (designated $T_{\rm sep}$) from the computed distribution of past times of close and slow encounters between the secondary and the primary. With the output frequency of 50 days we considered all possible clone combinations —it was 500×500 combinations for each primary–secondary couple— between the primary and the secondary and determined their physical distance $r_{\rm rel}$ and relative velocity $v_{\rm rel}$ at the encounter. Encounters satisfying the chosen distance and velocity limits were counted and their time histograms are shown in Figs. 1 to 13. The obtained number of close and slow encounters for each tested primary–secondary clone couple are given in brackets in the individual panels of the figures. The bin width of the histograms is 10 or 20 kyr for the past time axis spanning to < 1500 or ≥ 1500 kyr, respectively. Since the obtained distributions of $T_{\rm sep}$ are non-Gaussian and often strongly asymmetric, we used the median (i.e., the 50th percentile) value of the distribution as a nominal estimate for the time of separation of the given secondary from the primary (i.e., age estimate). For an uncertainty (error bar) of the separation time, we adopted the 5th and the 95th percentile of the distribution for the lower and upper limit on the separation time, respectively. We note that these $T_{\rm sep}$ allow us to assess whether the individual secondaries separated from the primary at same or different times.

In following subsections, we give details on the membership and age estimation for the individual clusters. In Table 1, we list the individual cluster members, their absolute magnitudes, distances from the primary and estimated ages.

[9] https://www.boulder.swri.edu/~hal/swift.html

2.1 (1270) Datura

The membership and the age estimate of ~ 500 kyr (uncertainty 50-100 kyr) for the cluster of (1270) Datura were obtained by Vokrouhlický et al. (2009, 2017). We use their rotation period and absolute magnitude data for the 17 members (including 4 one-opposition asteroids) they list, and we include 2 additional one-opposition asteroids 2015 PQ47 and 2016 TW15 with the corrected [10] absolute magnitudes $H = 19.4$ and 18.8, respectively, that are probable members of the cluster. While their orbits are still rather uncertain, the values of the longitude of node and perihelion match the expected location in the Datura family (see Fig. 12 of Vokrouhlický et al. 2017).

2.2 (2384) Schulhof

The membership and the age estimate of 800 ± 200 kyr for the cluster of (2384) Schulhof were obtained by Vokrouhlický et al. (2016). We use their primary rotation period and absolute magnitude data for the 12 members (including 4 one-opposition asteroids) they list, and we include 4 additional one-opposition asteroids 2013 GV46, 2016 EF9, 2016 EH195 and 2016 GY245 with the absolute magnitudes $H = 17.9, 17.5, 17.0$ and 17.0, respectively, that are probable members of the cluster. While their orbits are rather uncertain, we verified that they nominal realizations converge to that of (2384) Schulhof around the expected time $\simeq 800$ kyr.

2.3 (6825) Irvine

This cluster was discovered by Pravec and Vokrouhlický (2009). It consists of 4 members. The three secondaries were discovered in 2003–2005 and we checked that there are no other members among numbered and $\geq$ 2-opposition asteroids with $d_{\rm mean} < 100$ m/s from the primary in the current asteroid orbit catalog. Pravec and Vokrouhlický (2009) found that their orbits converged between 1.4 and 1.8 Myr before present and they noted that the three secondaries are somewhat displaced from the primary, suggesting that the three small asteroids could be "a cluster of fragments that were initially ejected with comparable velocity vectors". Indeed, we see that while the three secondaries have the distances from the primary $d_{\rm mean} = 57$ to 87 m/s, their mutual distances are 24 to 47 m/s, with the closest couple (143797) 2003 WA112 and (180233) 2003 UU192. Our backward integrations (Fig. 1) showed that while the largest secondary (143797) 2003 WA112 converged with the primary about 1370 kyr ago, the smallest secondary (236156) 2005 UL291 converged earlier, about 1930 kyr ago; there is almost no overlap between their clone encounter time distributions. The middle secondary (180233) 2003 UU192

[10] See Section 6.2 of Vokrouhlický et al. (2017) for the absolute magnitude correction procedure for Datura cluster members.

showed a broader clone encounter time distribution and it overlaps with both (143797) 2003 WA112 and (236156) 2005 UL291, though it is better consistent with the higher age of the latter. The method of clone convergences in the secular angles gave a formal age estimate of 1790^{+460}_{-350} kyr (see Electronic Supplementary Information). Both methods confirm the reality and the membership of this cluster.

2.4 (10321) Rampo

This cluster was discovered by Pravec and Vokrouhlický (2009). They found 3 members and estimated an age between 0.5 and 1.1 Myr. Recently there were discovered 4 other members during 2013–2016. Our backward orbital integrations (Fig. 2) showed that 4 of the 6 secondaries converged with the primary about 1400 kyr ago (uncertainty about $-500/+900$ kyr). (The low number of obtained encounters of the secondary 2015 HT91 with the primary is because this secondary's heliocentric orbit has a rather large uncertainty hyperellipsoid and we sampled it relatively sparsely with the limited number of orbital clones used.) Two secondaries, (294272) 2007 UM101 and 2016 TE87 have the time distributions of close encounters with the primary somewhat shifted to younger ages, with the median ages of 660 and 852 kyr, but they overlap with the distributions for the other four secondaries. It remains to be seen from future studies whether all the secondaries escaped from the primary at about the same time —perhaps between 900 and 1500 kyr ago where all the primary–secondary clone encounter time distributions overlap— or if the two secondaries mentioned above escaped later than the other four secondaries. The method of clone convergences in the secular angles gave a formal age estimate of 780^{+130}_{-90} kyr (see Electronic Supplementary Information). Both methods confirm the reality and the membership of this cluster.

2.5 (11842) Kap'bos

Pravec and Vokrouhlický (2009) identified the two asteroids (11842) Kap'bos and (228747) 2002 VH3 as apparently a significant pair. Pravec et al. (2010) estimated its age to be $\geq$ 150 kyr. We found that it is actually a cluster after the third member (436415) 2011 AW46 was discovered one year later. Our backward orbital integrations confirmed their membership and showed that the larger secondary (228747) converged with the primary 409^{+570}_{-248} kyr ago, while the smaller secondary has a possibility of recent convergence about 14 kyr ago (Fig. 3). We note that the distributions show a small overlap (see Fig. 4) that gives a possibility that the cluster's age might be perhaps in the range 100–500 kyr, but we leave an explanation of the only barely overlapping clone encounter time distributions for future study. We consider that the apparent possibility of a recent separation of the smaller secondary (436415) from the primary (11842) about 14 kyr ago may be just a result of synodic cycle approach of the two asteroids after their separation in the more

distant past (see Žižka et al. 2016 for discussion of this phenomenon). The method of clone convergences in the secular angles gave an age estimate of 420^{+410}_{-160} kyr (see Electronic Supplementary Information). The reality and the membership of this cluster are secure.

2.6 (14627) Emilkowalski

This cluster was discovered by Nesvorný and Vokrouhlický (2006). They found 3 members: (14627) Emilkowalski, (126761) 2002 DW10 and (224559) 2005 WU179. Nesvorný and Vokrouhlický (2006) used their orbits to find a possibility of their mutual convergence about 220 ± 30 ky ago, though they noted that the larger secondary's perihelion convergence was not perfect (see Fig. 2 of their paper). Later the fourth member of the cluster, (256124) 2006 UK337, was found and its convergence at about the proposed cluster age was checked. The apparent very young age of the cluster was a convenient starting point for an analysis of Emilkowalski's putative contribution to the interplanetary dust complex evidenced by dust bands. In particular, Vokrouhlický et al. (2008) noted that the young age of this cluster might imply that the associated, high-inclination band may be still incomplete. Indeed, Espy et al. (2009) and Espy Kehoe et al. (2015) used a fine analysis of the whole-sky IRAS observations to identify such a partial dust band at approximately 17° ecliptic latitude. According to results by Vokrouhlický et al. (2008) and Espy et al. (2009) this requires an age < 270 kyr.

We searched for potential new members of the Emilkowalski cluster in the current catalog of asteroid orbits. We found 3 asteroids, (434002) 2000 SM320, 2008 TN44 and (476673) 2014 UV143 that are somewhat more distant from the primary with $d_{\rm mean}$ from 104 to 120 m/s, but they are < 100 m/s from the largest secondary (126761) 2002 DW10 so they popped up as candidate members of the cluster. It is notable that the three small asteroids lie at mutual distances $d_{\rm mean} = 15$ to 18 m/s one from each other, forming a second core with a similar spread in the mean elements as the core of the 3 larger secondaries around the primary. We considered them as potential members of the cluster and checked their membership with backward orbital integrations (see below). We also found the single-opposition asteroid 2009 VF107 close to the cluster in the space of osculating orbital elements. While its orbit is too uncertain for an in-depth analysis, by numerically integrating its nominal (best-fit) orbit backward in time we verified convergence of the secular angles to those of (14627) Emilkowalski at about 1 Myr ago. This justifies to consider it a member of the cluster.

Our backward orbital integrations of all the six $\geq$ 2-opposition secondaries showed their past convergence with the primary, see Fig. 5. However, we have not found a single convergence time for all the six secondaries. Two secondaries, (256124) 2006 UK337 and (224559) 2005 WU179 apparently separated from the primary recently, about 320 kyr ago. (While the lower limit on their age of 230 kyr is well established, the upper limit is less well defined, see

Fig. 5b, c.) However, the other four secondaries show a convergence with the primary at times 1–4 Myr ago. The method of clone convergences in the secular angles gave age estimates of 300^{+40}_{-70} kyr and 1160^{+350}_{-160} kyr for the two groups of secondaries. (see Electronic Supplementary Information). Both methods confirm the membership of this cluster. The apparent cascade disruption of this cluster is very intriguing, but we leave it for a future study.

2.7 (16598) Brugmansia

The cluster of (16598) Brugmansia = 1992 YC2 consists of the primary asteroid accompanied by the two smaller asteroids (190603) 2000 UV80 and (218697) 2005 TT99. It was originally found by Nesvorný and Vokrouhlický (2006) who estimated an age of the cluster of 50–250 kyr. The two secondaries were discovered in 2000 and 2005 and we checked that there are no other members among numbered and $\geq$ 2-opposition asteroids with $d_{\rm mean} < 100$ m/s from the primary in the current asteroid orbit catalog. The times of convergence of clones of the cluster members in our backward integrations are shown in Fig. 6. The two distributions overlap nicely and they suggest that the secondaries separated from the primary about 170^{+60}_{-50} kyr ago. We checked also whether the asteroid (84329) 2002 TU51 that lies at a relatively large distance of $d_{\rm mean} = 87$ m/s from the primary belongs to the cluster, but we found no close encounters between their clones within the past 1 Myr. This indicates that (84329) is a nearby background asteroid and not a member of the cluster.

2.8 (18777) Hobson

This cluster was discovered by Pravec and Vokrouhlický (2009) and recently it was studied in detail by Rosaev and Plávalová (2017). They determined its age to 365 ± 67 kyr. On top of the members given by Rosaev and Plávalová (see their Tables 1 and 2), we found that additional small asteroids (450571) 2006 JH35, 2015 KA91 and 2014 OJ66 lie close to the cluster in the space of mean or osculating (for the latter two one-opposition asteroids) orbital elements. Our backward orbital integrations of the eight $\geq$ 2-opposition secondaries showed their past convergence with the primary, see Fig. 7. The close clone encounter time distributions for 7 of the 8 secondaries overlap well and they suggest an age of the cluster about 350 kyr, in agreement with the estimate by Rosaev and Plávalová (2017). While the lower limit on the cluster's age of 280 kyr appears well established (see Fig. 7c, e, f), the upper limit is less well defined. The secondary 2014 HH103 showed a weak convergence (small number of close and slow clone encounters with the primary in Fig. 7h), but this is probably because of a rather fast divergence of the limited number of clones used to sample the relatively large orbital uncertainty hyperellipsoid and range of the Yarkovsky drift of the small asteroid. We also verified that the nominal orbits of the one-opposition objects 2015 KA91 and 2014 OJ66 converge to that of (18777) Hobson around the time of the cluster formation,

thus we believe they are members of the cluster as well.

2.9 (20674) 1999 VT1

This cluster was discovered by Novaković et al. (2014) using the hierarchical clustering method in the space of proper elements. They found 9 members of the cluster, including the active asteroid P/2012 F5 (Gibbs), and estimated its age of 1.5 ± 0.1 Myr. In our search for asteroid pairs in the space of mean elements, 6 of the 8 inactive members found by Novaković et al. popped up as a significant cluster as well, with the closest couple (257134) 2008 GY132 and (321490) 2009 SH54 with $d_{\mathrm{mean}} = 7.6$ m/s, and there appeared a candidate 10th member (389622) 2011 HU90 that is at $d_{\mathrm{mean}} = 18$ m/s and $d_{\mathrm{prop}} = 1.1$ m/s from (341222) 2007 RT138. The only two cluster members that are distant (with d_{mean} between 300 and 500 m/s) in the space of mean elements from the core of the 7 closest members is the primary (20674) 1999 VT1 and the largest secondary (140429) 2001 TQ96. We run backward integrations of all the cluster members except the active asteroid P/2012 F5 and confirmed their membership (Fig. 8). Except for the largest secondary, the primary-secondary close encounter time distributions overlap within 0.1 Myr of 1.6 Myr, which is thus the age estimate for all but the largest secondary. The largest secondary (140429) 2001 TQ96 converged with the primary 3.0 Myr ago (with an uncertainty of about 0.6 Myr); the intriguing possibility of that it separated from the primary much earlier than the other secondaries remains open for future studies. The method of clone convergences in the secular angles gave a formal age estimate of 1560 ± 50 kyr for all but the largest secondary. (see Electronic Supplementary Information). The reality and the membership of this cluster are secure.

2.10 (21509) Lucascavin

This cluster was discovered by Nesvorný and Vokrouhlický (2006), they estimated its age to 300–800 kyr. It consists of 3 members. The two secondaries were discovered in 2003–2004 and we checked that there are no other members among numbered and $\geq$ 2-opposition asteroids with $d_{\mathrm{mean}} < 100$ m/s from the primary in the current asteroid orbit catalog. Our backward integrations (Fig. 9) showed that the larger secondary (180255) 2003 VM9 converged with the primary 370^{+640}_{-100} kyr ago, while the smaller secondary (209570) 2004 XL40 converged about 880^{+270}_{-370} kyr ago. While the distributions overlap so the cluster's age might be perhaps in the range 500–1000 kyr, we leave an explanation of the only partially overlapping clone encounter time distributions for future study.

We discovered this new cluster as a by-product of our search for asteroid pairs. The two asteroids (324154) 2005 YN176 and (459310) 2012 GZ32, which is the closest couple in this cluster with $d_{\rm mean} = 7.1$ m/s, popped up as a significant apparent couple and we found 2 more asteroids nearby, including the primary (22280) Mandragora. The distances of these three closest secondaries from the primary are $d_{\rm mean} < 35$ m/s. Then we found 6 more asteroids that are somewhat more distant from the primary with $d_{\rm mean}$ from 82 to 161 m/s, but they are < 100 m/s from some other secondaries so they popped up as candidate members of the cluster as well. These 9 "tight" secondaries are the first nine listed for the cluster in Table 1.

At that moment, the increasing number of secondaries with similar absolute magnitudes prompted us to perform further search for small, possibly related asteroids in a somewhat wider space around the (22280) Mandragora orbit. To that goal we employed the hierarchical clustering method (HCM) that is used for search of big (and mostly old) asteroid families in the space of proper orbital elements. We found 7 more candidate members associated with the cluster at velocity cutoffs between $45 - 65$ m/s. We also noted a difference between the velocity distance in the space of proper elements and $d_{\rm mean}$ from the primary in the space of mean elements that are 322 to 2094 m/s for these objects. The relatively large HCM velocity distance of these newly associated members, if compared to the escape velocity from a 10–15 km size parent body, and their large distances $d_{\rm mean}$ from the primary are most likely due to a proximity of the cluster to the major mean motion resonance J9/4 (see also below). The number of associated members in the HCM method stays small till the HCM velocity cutoff 75 m/s, where many asteroids from the same orbital zone collapse together. This is a practical expression of the local background distance level. Finally, we identified 2 more candidate members (265395) 2004 TM4 and 2010 RY26 that lie close to (204960) 4713 P-L in the space of mean elements (their distances are 13 and 31 m/s, respectively).

We run backward orbital integrations for all the 18 secondaries and we found that they all converged with the primary between 100 and 1000 kyr ago, thus confirming their membership to the cluster (see Figs. 10 and 11). We found that the orbits of the cluster members were affected by the nearby strong mean motion resonance J9/4 with Jupiter, resulting in the large distances of some of the secondaries from the primary and in their somewhat weak orbital convergences. (We also note that mean orbital elements for the members of this cluster have a bad quality with the Quality Code for Mean elements (QCM) of 4 in the AstDyS catalog, which is apparently an effect of the J9/4 resonance. This seems to explain the large $d_{\rm mean}$ values for some members of the cluster.) From the clone encounter time distributions of the 6 best converging secondaries (those with the numbers of clone encounters > 500 in Fig. 10), we estimate an age of the cluster of 250^{+290}_{-90} kyr. The method of clone convergences in the secular angles gave a formal age estimate of 290 ± 20 kyr (see Electronic Supplementary Information). Both methods confirm the reality of this cluster and the membership also appears secure even though the orbits

are affected by the nearby resonance J9/4.

2.12 (39991) Iochroma

This cluster was discovered by Pravec and Vokrouhlický (2009). It consists of 5 members. The four secondaries were discovered in 2005–2008 and we checked that there are no other members among numbered and $\geq$ 2-opposition asteroids with $d_{\rm mean} < 100$ m/s from the primary in the current asteroid orbit catalog. The times of convergence of clones of the cluster members in our backward integrations are shown in Fig. 12. The distributions overlap well and they suggest that the secondaries separated from (39991) about 190^{+200}_{-100} kyr ago. The method of clone convergences in the secular angles gave a formal age estimate of 140^{+130}_{-70} kyr (see Electronic Supplementary Information). The reality and the membership of this cluster are secure.

2.13 (66583) Nicandra

We discovered this new cluster as a by-product of our search for asteroid pairs. The two asteroids (279777) 1999 TT144 and 2014 QV272, which is the closest couple among $\geq$ 2-opposition asteroids in this cluster, popped up as a significant apparent couple with $d_{\rm mean} = 9.3$ m/s and we found one more multiple-opposition asteroid (66583) Nicandra nearby, which is the primary of the cluster. Moreover, we found two close one-opposition asteroids 2008 SO34 and 2012 TF228 that are probable members of the cluster too; the former is at a distance of 2 m/s only in the space of osculating orbital elements from (279777). With our backward orbital integrations we confirmed the membership of the three $\geq$ 2-opposition asteroids, see Fig. 13. An age of 870^{+170}_{-30} kyr is estimated from the clone encounters between (66583) and (279777). The secondary 2014 QV272 shows a relatively weak convergence (small number of close and slow clone encounters with the primary in Fig. 13b), but this is probably because of a rather fast divergence of the limited number of clones used to sample the relatively large orbital uncertainty hyperellipsoid and range of the Yarkovsky drift of the small asteroid. The method of clone convergences in the secular angles gave a formal age estimate of 890^{+210}_{-60} kyr (see Electronic Supplementary Information). Both methods confirm the reality and the membership of this cluster.

3 Sizes, mass ratios and primary rotations

The critical parameters that we need to know for the clusters are their primary periods and total secondary-to-primary mass ratios. We derived rotation periods of the primary members of the clusters from their photometric observations that we present in Electronic Supplementary Information.

The total secondary-to-primary mass ratio of an asteroid cluster is

$$q \equiv \sum_{j=2}^{N} q_j \equiv \frac{\sum_{j=2}^{N} M_j}{M_1}, \tag{3}$$

where M_j is a mass of the j-th component (1 for the primary, $2 \ldots N$ for the secondaries). We estimate the mass ratio q_j of the j-th secondary from the difference between its absolute magnitude H_j and the absolute magnitude of the primary H_1:

$$q_j = 10^{-0.6(H_j - H_1)}. \tag{4}$$

We also calculate the equivalent absolute magnitude of the secondaries $H_{\rm seceq}$ that is related to q as

$$q = 10^{-0.6(H_{\rm seceq} - H_1)}. \tag{5}$$

Note that $H_{\rm seceq}$ is the absolute magnitude of a body that would form if all the secondaries were put together to make single body.

The nominal values of the cluster parameters are given in Table 2. While uncertainties of the primary periods are mostly low and we do not give them in the table —they are reported in the subsections on individual objects below and in Electronic Supplementary Information—, we need to pay attention to uncertainties of the estimated mass ratios q.

We calculated the mass ratios using the primary absolute magnitudes that we derived from our precise photometric observations. However, absolute magnitudes for most of the secondaries were taken from the MPC catalog [11] and we assumed their standard errors 0.24 mag as found by Pravec et al. (2012; see their Table 3). We propagated the uncertainties of the absolute magnitudes and obtained uncertainties of the derived $\Delta H \equiv (H_{\rm seceq} - H_1)$ values that we report in Table 2. Uncertainties of the q values are obtained from the ΔH uncertainties using Eq. (5).

An additional uncertainty of the estimated mass ratios may arise from a possible incompletness of the known population (membership) of a given cluster; some small members may yet to be discovered. Thus, the calculated mass ratios

[11] http://www.minorplanetcenter.org/iau/MPCORB.html.

represent formally lower limits on true mass ratios of the clusters. Vokrouhlický et al. (2017) showed that the Datura cluster has a shallow size-frequency distribution, debiased the cluster's population and obtained an estimate for the true mass ratio $q = 0.045 \pm 0.009$, i.e., about twice as large as the mass ratio 0.021 that we calculated for the currently known members. We assume that the other clusters have shallow size-frequency distribution too. Another observation suggesting that the number of yet-to-be discovered secondaries is relatively small is the fact that for 6 of the 13 clusters we study, no new members were discovered during the last five years (since 2012) or longer while the recent sky surveys sampled the main belt asteroid population more thoroughly at fainter apparent magnitudes. This suggests that for nearly half of the clusters, there are no or only a relatively low number of small secondaries remaining to be discovered and that their currently known population (membership) is complete or effectively (for estimation of their ΔH and q) so. For the other 7 clusters where some small secondaries were discovered recently, we assume that their population incompletness is similar to that of the cluster of Datura and we adopt asymmetric error bars for their ΔH values with a lower uncertainty value of -0.6 mag that corresponds to the factor of 0.045/0.021 mass ratio incompletness estimated for the population of Datura, rounded to the nearest tenth (see Table 2).

An error of the opposite sign —leading to overestimation of the mass ratio– could occur if some of the identified asteroids were not real members of a given cluster, but they were interlopers. We consider a possible uncertainty caused by this effect being low. Most cluster members are secure as we found with the orbital integrations in Section 2. Some cases with weak orbital convergences discussed in Section 2 may not be entirely secure identifications, but they are generally small asteroids and their contribution to the total mass of the secondaries of given cluster is low, thus a possible error in the calculated mass ratio is small. We neglect this minor uncertainty.

As an additional information, we obtained or estimated diameters (D_1) and geometric albedos ($p_{V,1}$) of the cluster primaries. For 7 of the 13 primaries, we took the diameters and geometric albedos from their WISE observations (Masiero et al. 2011) and refined them using our accurate H_1 values using the method described in Pravec et al. (2012). Uncertainties of the refined D_1 and $p_{V,1}$ values are about 10% and 20-25%, respectively, unless other values are reported below. For the remaining 6 primaries where no thermal WISE observations were obtained, we estimated their diameters assuming the mean geometric albedos for their probable spectral types.

We give details and references for the parameters of the individual clusters in following subsections.

3.1 (1270) Datura

Vokrouhlický et al. (2009, 2017) obtained following values for the parameters of (1270) Datura. The primary rotation period $P_1 = 3.358100 \pm 0.000003$ h

and the mean observed lightcurve amplitude $\mathcal{A}_1 = 0.50$ mag. The primary mean absolute magnitude $H_1 = 12.65 \pm 0.05$. The primary effective diameter $D_1 = 8.2$ km and the geometric albedo $p_{V,1} = 0.24$, refined from the WISE measurements using the accurate absolute magnitude value.

3.2 (2384) Schulhof and (81337) 2000 GP36

Vokrouhlický et al. (2016) obtained $P_1 = 3.293677 \pm 0.000002$ h, $\mathcal{A}_1 = 0.39$ mag, $H_1 = 12.13 \pm 0.06$, $D_1 = 11.6$ km and $p_{V,1} = 0.19 \pm 0.04$.

We observed the largest secondary of this cluster (81337) 2000 GP36 from Maidanak on three nights during 2014 August 24 to September 1 and from Rozhen on two nights 2015 November 13 and 14. We obtained its period $P_2 = 10.028 \pm 0.001$ h in 2014 and 10.027 ± 0.006 h in 2015, with lightcurve amplitudes $\mathcal{A}_2 = 1.22$ and 1.36 mag at solar phases 6–9° and 11°, respectively. The mean absolute magnitude $H_2 = 15.39 \pm 0.06$ was derived (see Electronic Supplementary Information).

3.3 (6825) Irvine and (143797) 2003 WA112

From our photometric observations (see Electronic Supplementary Information), we obtained following parameters for (6825) Irvine. The primary rotation period $P_1 = 3.61589 \pm 0.00005$ h and the lightcurve amplitude $\mathcal{A}_1 = 0.58$ mag at the lowest observed solar phase 5°. The mean absolute magnitude $H_1 = 14.07 \pm 0.15$, derived assuming $G_1 = 0.24 \pm 0.11$ and $(V-R)_1 = 0.49 \pm 0.05$ that are the mean values for S types (which is a likely spectral type of Irvine, for its moderate albedo and position in the inner main belt; see also $(V-R)_2$ below). The primary effective diameter $D_1 = 4.6$ km and the geometric albedo $p_{V,1} = 0.20$, refined from the WISE measurements using the accurate absolute magnitude value.

We observed the largest secondary of this cluster (143797) 2003 WA112 with the 1.54-m telescope at La Silla on two nights 2017 January 2 and 3. We could not derive its period because of its low amplitude that we estimate $\mathcal{A}_2 \approx 0.02$ mag. The color index in the Johnson-Cousins photometric system $(V-R)_2 = 0.477 \pm 0.016$, consistent with its likely S type classification (see also the previous paragraph). The mean absolute magnitude $H_2 = 16.62 \pm 0.05$, derived assuming $G_2 = 0.24 \pm 0.11$ (the mean value for S types).

3.4 (10321) Rampo

From our photometric observations (see Electronic Supplementary Information), we obtained following parameters for (10321) Rampo. The primary ro-

tation period $P_1 = 5.2282 \pm 0.0007$ h and the lightcurve amplitude $\mathcal{A}_1 = 0.69$ mag measured on 2013 January 9 and 10 when the asteroid was observed at lower asterocentric latitudes (see Electronic Supplementary Information for details). The color index in the Johnson-Cousins photometric system $(V-R)_1 = 0.500 \pm 0.010$, consistent with an S type classification that is likely for Rampo, considering also its moderate albedo and position in the inner main belt. The mean absolute magnitude $H_1 = 14.60 \pm 0.09$, derived assuming $G_1 = 0.24 \pm 0.11$ (the mean value for S types). The primary effective diameter $D_1 = 3.8$ km and the geometric albedo $p_{V,1} = 0.18$, refined from the WISE measurements using the accurate absolute magnitude value.

3.5 (11842) Kap'bos and (228747) 2002 VH3

Pravec et al. (2010) measured the primary rotation period $P_1 = 3.68578 \pm 0.00009$ h. The mean lightcurve amplitude $\mathcal{A}_1 = 0.13$ mag observed at solar phases 3–21° (see Electronic Supplementary Information for details). The color index in the Johnson-Cousins photometric system $(V-R)_1 = 0.460 \pm 0.012$, consistent with an S type classification that is likely for Kap'bos as it lies in the Flora family. The mean absolute magnitude $H_1 = 14.42 \pm 0.03$, derived assuming $G_1 = 0.24 \pm 0.11$ (the mean value for S types). An effective diameter D_1 of about 4 km was estimated from the absolute magnitude, assuming $p_{V,1} = 0.20$ that is the mean geometric albedo for S types (Pravec et al. 2012).

We observed the largest secondary of this cluster (228747) 2002 VH3 with the 1.54-m telescope at La Silla on ten nights during 2017 January 19 to February 3. We found the rotation period $P_2 = 7.961 \pm 0.002$ h and the lightcurve amplitude $\mathcal{A}_2 = 0.20$ mag at solar phases 6–13° The color index in the Johnson-Cousins photometric system $(V-R)_2 = 0.497 \pm 0.019$, consistent with its probable S type classification (see the previous paragraph). The mean absolute magnitude $H_2 = 17.16 \pm 0.04$ and the phase relation's slope parameter $G_2 = 0.34 \pm 0.06$.

3.6 (14627) Emilkowalski

From our photometric observations (see Electronic Supplementary Information), we obtained following parameters for (14627) Emilkowalski. The primary rotation period $P_1 = 11.1313 \pm 0.0009$ h. The lightcurve amplitude $\mathcal{A}_1 = 0.67$ mag observed at solar phase 12°. The mean absolute magnitude $H_1 = 13.61 \pm 0.06$ and the phase relation's slope parameter $G_1 = -0.05 \pm 0.03$, derived assuming $(V-R)_1 = 0.455 \pm 0.033$ that is the mean color index for D types (Pravec et al. 2012), which is a proposed classification for this asteroid by Vereš et al. (2015). The primary effective diameter $D_1 = 6.9$ km and the geometric albedo $p_{V,1} = 0.13$, refined from the WISE measurements using the accurate absolute magnitude value.

3.7 (16598) Brugmansia

From our photometric observations (see Electronic Supplementary Information), we obtained following parameters for (16598) Brugmansia. The primary rotation period $P_1 = 3.9272 \pm 0.0003$ h, with the lightcurve amplitude $\mathcal{A}_1 = 0.37$ and 0.30 mag in 2009 and 2013, respectively. The mean absolute magnitude $H_1 = 14.69 \pm 0.26$, derived assuming $G_1 = 0.15 \pm 0.20$ and $(V-R)_1 = 0.45 \pm 0.10$. An effective diameter D_1 of about 5 km was estimated from the absolute magnitude, assuming $p_{V,1} = 0.10$. The relatively large uncertainty of the H_1 and the assumed G_1, color index and albedo values are due to an unconstrained taxonomic type of this asteroid; the assumed values are the means or defaults for the entire main belt asteroid population.

3.8 (18777) Hobson and (57738) 2001 UZ160

From our photometric observations (see Electronic Supplementary Information), we obtained following parameters for (18777) Hobson. The primary rotation period $P_1 = 10.227 \pm 0.004$ h. The lightcurve amplitude $\mathcal{A}_1 = 0.21$ mag observed at solar phase 4°. The color index in the Johnson-Cousins photometric system $(V-R)_1 = 0.477 \pm 0.010$, consistent with a S type that is typical for asteroids in the given part of the main belt. The mean absolute magnitude $H_1 = 15.16 \pm 0.05$ and the phase relation's slope parameter $G_1 = 0.08 \pm 0.10$. An effective diameter D_1 of about 3 km was estimated from the absolute magnitude, assuming $p_{V,1} = 0.20$ that is the mean geometric albedo for S types (Pravec et al. 2012).

We observed the large secondary (57738) 2001 UZ160 with the 1.54-m telescope at La Silla on four nights from 2013 October 26 to November 5 and with the 2.6-m telescope at Nauchny on night 2013 November 6. We found the rotation period $P_2 = 20.51 \pm 0.01$ h and the lightcurve amplitude $\mathcal{A}_2 = 0.65$ mag at solar phase 4°. The color index in the Johnson-Cousins photometric system $(V-R)_2 = 0.46 \pm 0.02$ that agrees with the primary's color index. The mean absolute magnitude $H_2 = 15.41 \pm 0.05$, derived assuming the primary's $G = 0.08 \pm 0.10$.

3.9 (20674) 1999 VT1, (140429) 2001 TQ96, (177075) 2003 FR36 and (249738) 2000 SB159

From our photometric observations (see Electronic Supplementary Information), we obtained following parameters for (20674) 1999 VT1. The primary rotation period $P_1 = 6.311 \pm 0.001$ h and the lightcurve amplitude $\mathcal{A}_1 = 0.78$ mag. The mean absolute magnitude $H_1 = 12.81 \pm 0.06$, derived assuming $G_1 = 0.12 \pm 0.08$ and $(V-R)_1 = 0.38 \pm 0.05$ (the defaults for C types). An effective diameter D_1 of about 12 km was estimated from the absolute

magnitude, assuming $p_{V,1} = 0.10$.

We observed the largest secondary of this cluster (140429) 2001 TQ96 with the 1.54-m telescope at La Silla on four nights 2016 October 25 to 28. We found a probable rotation period of $P_2 = 39.8 \pm 0.7$ h, derived assuming two pairs of maxima/minima per period, with the lightcurve amplitude $\mathcal{A}_2 = 0.19$ mag at solar phase 18°. The mean absolute magnitude $H_2 = 15.19 \pm 0.11$, derived assuming $G_2 = 0.12 \pm 0.08$ and $(V - R)_2 = 0.38 \pm 0.05$ (the defaults for C types).

We observed the secondary (177075) 2003 FR36 with the 1.54-m telescope at La Silla on nine nights from 2016 October 31 to November 9. We found the rotation period $P = 6.818 \pm 0.003$ h and the lightcurve amplitude $\mathcal{A} = 0.37$ mag at solar phase 4°. The mean absolute magnitude $H = 15.88 \pm 0.06$, derived assuming $G = 0.12 \pm 0.08$ and $(V - R) = 0.38 \pm 0.05$ (the defaults for C types).

We observed the secondary (249738) 2000 SB159 with the 1.54-m telescope at La Silla on nine nights from 2016 October 31 to November 9. We found a likely rotation period of $P = 41.2 \pm 0.5$ h and the lightcurve amplitude $\mathcal{A} = 0.11$ mag at solar phase 6°. The mean absolute magnitude $H = 15.96 \pm 0.06$, derived assuming $G = 0.12 \pm 0.08$ and $(V - R) = 0.38 \pm 0.05$ (the defaults for C types).

3.10 (21509) Lucascavin

From our photometric observations (see Electronic Supplementary Information), we obtained following parameters for (21509) Lucascavin. The primary rotation period $P_1 = 5.7891 \pm 0.0008$ h and the lightcurve amplitude $\mathcal{A}_1 = 0.23$–0.30 mag. The color index in the Johnson-Cousins photometric system $(V - R)_1 = 0.474 \pm 0.016$, consistent with an S type classification that is likely for this asteroid. The mean absolute magnitude $H_1 = 15.15 \pm 0.07$, derived assuming $G_1 = 0.24 \pm 0.11$ (the mean value for S types). An effective diameter D_1 of about 3 km was estimated from the absolute magnitude, assuming $p_{V,1} = 0.20$ that is the mean geometric albedo for S types (Pravec et al. 2012).

3.11 (22280) Mandragora and (43239) 2000 AK238

From our photometric observations (see Electronic Supplementary Information), we obtained following parameters for (22280) Mandragora. The probable primary rotation period $P_1 = 28.48 \pm 0.03$ h (see Electronic Supplementary Information) and the lightcurve amplitude $\mathcal{A}_1 = 0.09$ mag. The color index in the Johnson-Cousins photometric system $(V - R)_1 = 0.405 \pm 0.012$. The mean absolute magnitude $H_1 = 14.02 \pm 0.07$ and the phase relation slope parameter $G_1 = 0.07 \pm 0.05$. The primary effective diameter $D_1 = 9.8$ km and the

geometric albedo $p_{V,1} = 0.045 \pm 0.010$, refined from the WISE measurements using the accurate absolute magnitude value.

We observed the largest secondary of this cluster (43239) 2000 AK238 with the 1.54-m telescope at La Silla on five nights during 2017 January 25 to February 3. We found the rotation period $P_2 = 15.825 \pm 0.009$ h and the lightcurve amplitude $\mathcal{A}_2 = 0.34$ mag at solar phase 8°. The color index in the Johnson-Cousins photometric system $(V-R)_2 = 0.396 \pm 0.017$. The mean absolute magnitude $H_2 = 14.90 \pm 0.04$, assuming the primary's slope parameter $G = 0.07 \pm 0.05$. The effective diameter $D_2 = 6.5$ km and the geometric albedo $p_{V,2} = 0.045 \pm 0.014$, refined from the WISE measurements using the accurate absolute magnitude value. We note the excellent agreement between the color indices and geometric albedos of the primary and the secondary, which further strengthens their genetic relation inferred from the orbital analysis in Section 2.11.

3.12 (39991) Iochroma and (340225) 2006 BR54

From our photometric observations (see Electronic Supplementary Information), we obtained following parameters for (39991) Iochroma. The primary rotation period $P_1 = 3.440 \pm 0.002$ h and the lightcurve amplitude $\mathcal{A}_1 = 0.37$ mag at solar phase 4°. The color index in the Johnson-Cousins photometric system $(V-R)_1 = 0.510 \pm 0.012$, consistent with an S type classification that is likely for this asteroid. The mean absolute magnitude $H_1 = 14.79 \pm 0.14$, derived assuming $G_1 = 0.24 \pm 0.11$ (the mean value for S types). An effective diameter D_1 of about 3 km was estimated from the absolute magnitude, assuming $p_{V,1} = 0.20$ that is the mean geometric albedo for S types.

We observed the secondary (340225) 2006 BR54 with the 1.54-m telescope at La Silla on five nights during 2016 November 30 to December 7. We found the rotation period $P = 8.869 \pm 0.005$ h and the lightcurve amplitude $\mathcal{A} = 0.50$ mag at solar phase 5°. The mean absolute R magnitude $H_R = 17.71 \pm 0.05$ that converts to $H = 18.20 \pm 0.07$, assuming $G = 0.24 \pm 0.11$ and $(V-R) = 0.49 \pm 0.05$ that are the mean values for S types (see Pravec et al. 2012).

3.13 (66583) Nicandra and (279777) 1999 TT144

From our photometric observations (see Electronic Supplementary Information), we obtained following parameters for (66583) Nicandra. The primary rotation period $P_1 = 6.457 \pm 0.001$ h or twice that (see Electronic Supplementary Information) and the lightcurve amplitude $\mathcal{A}_1 = 0.07$ mag. The color index in the Johnson-Cousins photometric system $(V-R)_1 = 0.355 \pm 0.01$. The mean absolute magnitude $H_1 = 14.91 \pm 0.14$ and the phase relation's slope parameter $G_1 = 0.01 \pm 0.08$. The primary effective diameter $D_1 = 6.0$ km and the geometric albedo $p_{V,1} = 0.053$, refined from the WISE measurements using

the accurate absolute magnitude value.

We observed the largest secondary of this cluster (279777) 1999 TT144 with the 1.54-m telescope at La Silla on three nights 2016 October 6–8. We found the rotation period $P_2 = 6.517 \pm 0.007$ h and the lightcurve amplitude $\mathcal{A}_2 = 0.55$ mag at solar phase 18°. The color index in the Johnson-Cousins photometric system $(V-R)_2 = 0.359 \pm 0.017$, in excellent agreement with the primary's color index. The mean absolute magnitude $H_2 = 16.46 \pm 0.11$, assuming the primary's $G = 0.01 \pm 0.08$.

4 Fission mechanics

We compare the asteroid cluster data with predictions from the theory of asteroid rotational fission first proposed in Scheeres (2004, 2007) and applied to asteroid pairs by Pravec et al. (2010). In this and the next section, we provide an overview of the fission mechanics and apply the basic model from Pravec et al. (2010, The Supplementary Information Section 4) to generalize the fission theory to a system consisting of an arbitrary number of secondaries.

Rotating bodies can be characterized by their total energy and rotational angular momentum. When the body is a single entity, the rotational angular momentum vector is simply computed as

$$\boldsymbol{L} = \boldsymbol{I} \cdot \boldsymbol{\omega}, \tag{6}$$

where $\boldsymbol{I}$ is the rotational inertia tensor and $\boldsymbol{\omega}$ is the angular velocity of the body. The total energy of a rotating body is also driven by its rotation rate, but is also a function of its mass distribution through its self-potential ($\mathcal{U}$):

$$E = \frac{1}{2}\boldsymbol{\omega} \cdot \boldsymbol{I} \cdot \boldsymbol{\omega} + \mathcal{U}. \tag{7}$$

The rotational inertia tensor and the self-potential are defined through the mass distribution of the body:

$$\boldsymbol{I} = \int\limits_{\beta} \left[(\boldsymbol{r} \cdot \boldsymbol{r})\, \boldsymbol{U} - \boldsymbol{r}\boldsymbol{r} \right] dm, \tag{8}$$

$$\mathcal{U} = -\frac{G}{2} \int\limits_{\beta} \int\limits_{\beta} \frac{dm dm'}{|\boldsymbol{r} - \boldsymbol{r}'|}, \tag{9}$$

where β represents the mass distribution, $\boldsymbol{U}$ is the identity dyad, $\boldsymbol{r}, \boldsymbol{r}'$ is the location in the body of a mass element dm, dm', and G is the gravitational constant.

As a rubble-pile body undergoes changes in its rotation rate (e.g., as a result of spin-up of the body by the YORP effect), the mass distribution parameters can remain constant over a relatively wide range of rates, unlike a fluidic body which will change its shape incrementally with changes in total angular momentum. Despite this, if the total angular momentum of the object becomes large enough, even collections of rigid components can undergo shifts into configurations that have a lower total energy, with excess energy being dissipated thermally or through seismic waves (Scheeres 2007).

As the angular momentum of the body increases, eventually the minimum energy configuration for the body can involve components of the body entering orbit about each other (Scheeres 2007, 2009). The transition from a collection of rigid components resting on each other to one where N of the collections

are in mutual orbit liberates potential energy that can then drive the system dynamically.

Here we consider a rubble pile body that undergoes such a fission event, nominally conserving its energy across fission [12] and decomposing it into multiple components that then enter orbit about each other, splitting the initial energy in Eq. (7) into mutual and self kinetic and potential interactions between the components (Scheeres 2017):

$$E = \sum_{j=1}^{N} \frac{1}{2} \boldsymbol{\omega_c} \cdot \boldsymbol{I}_j \cdot \boldsymbol{\omega_c} + \frac{1}{2\ M} \sum_{i=1}^{N-1} \sum_{j=i+1}^{N} M_i M_j \boldsymbol{v}_{ij} \cdot \boldsymbol{v}_{ij} + \sum_{i,j=1}^{N} \mathcal{U}_{ij}, \tag{10}$$

where $\boldsymbol{\omega_c}$ is the critical spin rate at which the body disassociates, M is the total mass of the system, M_j and I_j are the mass and inertia dyad of body j, $\boldsymbol{v}_{ij}$ is the relative velocity between components i and j, $\mathcal{U}_{ii}$ is the self-potential of the new components and $\mathcal{U}_{ij} + \mathcal{U}_{ji}$ is the mutual potential between the components i and j, where

$$\mathcal{U}_{ij} = -\frac{G}{2} \int_{\beta_i} \int_{\beta_j} \frac{dm_i dm_j}{|\boldsymbol{r}_i - \boldsymbol{r}_j|}. \tag{11}$$

The mutual potential represents a conduit for energy being transferred from rotational to translational energy and vice-versa. For these initial conditions we note that $v_{ij}^2 \sim \omega^2 r_{ij}^2$ as the initial motion is just due to relative rotation. We also note that the mutual potential can be approximated as $2\mathcal{U}_{ij} \sim -\frac{GM_iM_j}{r_{ij}}$.

The free energy of the system is defined as the total energy minus the self-potentials $\mathcal{U}_{ii}$, and if this is positive the system can undergo complete escape of all components (Scheeres 2002, 2016). Assuming a positive free energy, if the bodies all mutually escape with $v_{\infty ij}^2$ the relative velocity between the bodies i and j at infinity and $\boldsymbol{\omega}_j$ the angular velocity of the body j, the mutual potentials all go to zero, leaving the free energy as

$$E_{free} = \sum_{j=1}^{N} \frac{1}{2} \boldsymbol{\omega}_j \cdot \boldsymbol{I}_j \cdot \boldsymbol{\omega}_j + \frac{1}{2\ M} \sum_{i=1}^{N-1} \sum_{j=i+1}^{N} M_i M_j v_{\infty ij}^2 \tag{12}$$

and consisting only of kinetic energies.

The post-fission distribution of energy can ideally be balanced with the post-escape energies. Furthermore, for most of our studied systems we can assume that the mass of the primary body dominates over the other bodies, i.e., $M_j \ll M_1$, $j = 2, 3, \ldots, N$. This allows us to equate the two energies and rewrite the summations as

[12] If weak cohesive forces are accounted for between rubble pile components, the overall spin rate for fission will be increased, with the change being small for bodies greater than a few kilometers.

$$\frac{1}{2}\omega^2 I_1 + \mathcal{O}(M_j^{5/3})_{j\geq 2} + \frac{M_1}{M}\sum_{j=2}^{N} M_j r_{1j}^2 \left[\frac{1}{2}\omega^2 - \frac{GM}{r_{1j}^3}\right] + \mathcal{O}(M_j M_k)_{j,k\geq 2} = \frac{1}{2}\omega_\infty^2 I_1 + \mathcal{O}(M_j^{5/3})_{j\geq 2} + \frac{M_1}{2\ M}\sum_{j=2}^{N} M_j v_{\infty 1j}^2 + \mathcal{O}(M_j M_k)_{j,k\geq 2}. \quad (13)$$

With our assumption that M_1 is relatively large, the products of all M_j, $j \neq 1$ will be relatively small, allowing us to ignore them to the leading order. Thus all of the $O()$ terms can be neglected. We can also note that the moments of inertia go as $M_j^{5/3}$ and thus that they will also be negligible with respect to $M_1 M_j$, justifying our neglect.

We assume that $r_{1j} \sim R$, defining a system that starts with the mass elements equidistant from the largest primary. We also characterize the initial spin state as $\omega^2 = \alpha_L^2 \frac{GM}{R^3}$, where α_L is a scaling factor previously introduced in Pravec and Harris (2007) that expresses the proximity of the body to the critical angular momentum, and which can also be used to parameterize the spin rate relative to the circular velocity rate on the surface of the total body. Finally, note that the mass $\sum_{j=2}^{N} M_j \equiv M - M_1$. We also note $v_\infty^2 \geq 0$ to find the inequality

$$\frac{1}{2}\alpha_L^2 \frac{GM}{R^3} I_1 - \frac{GM_1}{2R}(M - M_1) \geq \frac{1}{2}\omega_{1,\infty}^2 I_1. \quad (14)$$

Dividing by $I_1/2$ gives the inequality

$$\alpha_L^2 \frac{GM}{R^3} - \frac{GM_1(M - M_1)}{RI_1} \geq \omega_{1,\infty}^2 \quad (15)$$

which can be used for constraining the final rotation rate of the primary.

With $M_j \ll M_1, j = 2, 3, \ldots, N$, the radii of an individual secondary component is small compared to the radius of the primary and we approximate $R \sim R_1$. If we also assume a spherical shape for the initial body, $I_1 = 2M_1 R^2/5$ and its critical rotation, i.e., $\alpha_L = 1$, we can express a hard limit between the final primary spin rate and the ejected mass loss

$$\omega_{1,\infty}^2 \leq \frac{4\pi}{3} G\rho \left[1 - \frac{5}{2}\frac{M - M_1}{M}\right] \equiv \frac{4\pi}{3} G\rho \left[1 - \frac{5}{2(1 + q^{-1})}\right]. \quad (16)$$

We point out that this relation —implying that asteroid pairs and clusters formed by rotational fission must have $q \leq 2/3$— represents a theoretical hard limit and that for real systems the final primary spin rates may be more confined (see the last paragraph of section 5).

Being equipped with the results of the theory of fission mechanics, we constructed a simple model of the post-fission system, analogous to the model of Pravec et al. (2010) for asteroid pairs, that we will use for interpretation of a relation between the spin rates of asteroid cluster primaries and the cluster

mass ratios. The model, its assumptions and mathematical formulation are given in the next section.

5 Model of a proto-system separation

To quantify our asteroid clusters we model the post-fission system as a system of N components starting in close proximity and with the total angular momentum in the range of critical values as observed in close binary systems (Pravec and Harris, 2007). Assuming the mass distribution in the components of the system is fixed in this post-fission evolution phase, the free energy of the system is constant. Energy is transferred between the rotational and orbital energy by a conduit of the mutual potentials between the components. The model is following:

- Most of the system's mass is contained in the largest (primary) body, i.e., $q \equiv \sum_{j=2}^{N} q_j \equiv \sum_{j=2}^{N} M_j/M_1 \ll 1$.
- The initial state is a close system of N orbiting components.
- The end state is with barely escaping satellites (parabolic orbits).
- Both the free energy and the total angular momentum of the system are conserved.
- The total angular momentum is close to critical ($\alpha_L \sim 1$), as we observe in small binary systems (Pravec and Harris, 2007).
- The system is coplanar, i.e., rotation and orbit poles are aligned. The rotations are prograde and around the principal axes of the bodies.
- We assume constant secondary periods, neglecting possible changes in the secondaries' rotational angular momenta due to their small sizes.
- Bulk density of the components is $\rho = 2$ g/cm^3.

The first six assumptions are fundamental, whereas the last two ones are less critical as outcomes of the model are less sensitive to variations of these parameters within observed or plausible ranges.

The mathematical formulation of our model follows. As $q \ll 1$, the free energy of the system is approximated as

$$E_{\text{Free}} \doteq \frac{1}{2} I_1 \omega_1^2 + \sum_{j=2}^{N} \left(\frac{1}{2} I_j \omega_j^2 - G \frac{M_1 M_j}{2A_j} \right), \tag{17}$$

where I_i, ω_i, M_i are the moment of inertia around the principal axis, the angular velocity and the mass of the i-th body (1 for the primary, 2 to N for the secondaries), respectively, and A_j is the semimajor axis of the j-th body's orbit around the primary.

Since the free energy and ω_j for $j = 2, \ldots N$ are constant, we get

$$\frac{1}{2} I_1 \omega_{1,\text{ini}}^2 - \sum_{j=2}^{N} G \frac{M_1 M_j}{2A_{j,\text{ini}}} = \frac{1}{2} I_1 \omega_{1,\text{final}}^2, \tag{18}$$

where the subscripts "ini" and "final" denote initial and end state values of the parameters. Note that $1/A_{j,\mathrm{final}} = 0$ for the end state of a barely escaping satellite (parabolic orbit).

We assume that the secondaries were initially on the same distance from the primary, $A_{j,\mathrm{ini}} = A_{\mathrm{ini}}$ for $j = 2, \ldots N$.

$$\frac{1}{2} I_1 \omega_{1,\mathrm{ini}}^2 - G \frac{M_1 \sum_{j=2}^{N} M_j}{2A_{\mathrm{ini}}} = \frac{1}{2} I_1 \omega_{1,\mathrm{final}}^2. \tag{19}$$

In Eq. (19), we substitute $\sum_{j=2}^{N} M_j \equiv \sum_{j=2}^{N} q_j M_1 \equiv q M_1$ (from Eq. (3)), the moment of inertia of the primary

$$I_1 = \frac{M_1}{5}(a_1^2 + b_1^2) \tag{20}$$

and $M_1 = V_1 \rho$, where V_1 is the volume of the primary. We assume that V_1 is equal to the volume of the dynamically equivalent equal mass ellipsoid (DEEME) of the primary, i.e., $V_1 = a_1 b_1 c_1 \pi 4/3$. The parameters a_1, b_1, c_1 are semiaxes of the DEEME of the primary. After the substitutions, we get

$$\omega_{1,\mathrm{final}}^2 = \omega_{1,\mathrm{ini}}^2 - \frac{\frac{20}{3}\pi q G \frac{a_1}{b_1}\frac{c_1}{b_1}\rho}{\left[1 + \left(\frac{a_1}{b_1}\right)^2\right]\frac{A_{\mathrm{ini}}}{b_1}}. \tag{21}$$

We note that this Eq. (21) is identical to Eq. (15) in the Supplementary Information of the paper Pravec et al. (2010), with the mass ratio $q \equiv \sum_{j=2}^{N} q_j \equiv \sum_{j=2}^{N} M_j/M_1$ having $N = 2$ for an asteroid pair and $N > 2$ for an asteroid cluster. The initial angular velocity of the primary $\omega_{1,\mathrm{ini}}$ is estimated from the normalized total angular momentum of the system in a way as described in Section 5 of the Supplementary Information of Pravec et al. (2010).

We calculated asteroid cluster primary's final rotation periods as functions of mass ratio q for the same sets of parameters as we used for asteroid pairs in Pravec et al. (2010). With the adopted approximations, the functions are virtually identical to those we obtained for asteroid pairs. We plot them in Fig. 14 together with the data for asteroid clusters from Table 2 and our up-to-date data for 93 asteroid pairs (an update of the asteroid pairs data set of Pravec et al. 2010; we prepare it for publication after completing our current observational project on asteroid pairs in 2017). Specifically, the black dashed curve is for the normalized total angular momentum of the system $\alpha_L = 1.0$, the primary's equatorial elongation $a_1/b_1 = 1.4$, $b_1/c_1 = 1.2$, and the initial relative semi-major axis $A_{\mathrm{ini}}/b_1 = 3$. This set of parameters can be considered as the best representation of pair and cluster parameters. In particular, the total angular momentum content of 1.0 is about the mean of the distribution of α_L values in small binaries (Pravec and Harris 2007), and the axial ratio of 1.4 is about a mean of equatorial elongations of pair and cluster primaries suggested by their observed amplitudes. The red and blue

curves represent upper and lower limit cases. The upper curves are for the system's normalized total angular mometum $\alpha_L = 1.2$, primary's axial ratio $a_1/b_1 = 1.2$, and initial orbit's normalized semi-major axis $A_{\rm ini}/b_1 = 2$ and 4. The lower curves are for $\alpha_L = 0.7, a_1/b_1 = 1.5$ and $A_{\rm ini}/b_1 = 2$ and 4. The choice of $a_1/b_1 = 1.2$ for the upper limit cases is because the asteroid pair primaries closest to the upper limit curve have low amplitudes $\mathcal{A}_1 =$ 0.1–0.2 mag. Similarly, the choice of $a_1/b_1 = 1.5$ for the lower limit cases is because the highest amplitudes of the points close to the lower limit curve are $\mathcal{A}_1 = 0.4$–0.5 mag, suggesting the equatorial elongations $\sim$ 1.4–1.5. For completness, the green curve gives the theoretical hard upper limit on the final primary spin rate (i.e., lower limit on the period) derived in the previous section (Eq. (16)). We point out that the theoretical hard limit was derived involving certain idealizations that are probably not fulfilled in real asteroids. In particular, it assumes spherical component shapes while real asteroids are non-spherical. Thus, real asteroid pairs (and clusters) formed by spin-up fission may stay well below the theoretical hard limit. Indeed, we see in Fig. 14 that the observed asteroid pairs do not extend to the green curve at q about 0.6, but they are well to the right of the curve (except for the group of four anomalous high-mass ratio pairs in the upper left of the plot, which require an additional source of angular momentum for their separation; this will be discussed in a future paper). Our model of a proto-system separation described in this section provides a good fit to the data and it appears to be more realistic.

6 Cluster formation by rotational fission

The agreement of our asteroid cluster data with the prediction from the theory of rotational fission shown in Fig. 14 is excellent for 11 of the 13 clusters. The two exceptions are the high-mass ratio clusters of (18777) Hobson and (22280) Mandragora. With their q about 1.01 and 0.73, or greater, they are not consistent with being formed solely by rotational fission, and an additional source of angular momentum is needed. Alternatively, these two clusters could have been formed by collisions, like larger and older asteroid families. The properties of the other 11 clusters are consistent with the hypothesis that they were formed by rotational fission.

A candidate mechanism for formation of more than one secondary after a primary rotational fission event is the secondary fission process proposed by Jacobson and Scheeres (2011). Secondary fission is a rotational fission of the secondary induced via spin–orbit coupling and occurring during the chaotic binary stage. The mechanism is proposed to work as follows: First, a parent asteroid fissions and a proto-binary system is formed. Spin–orbit coupling transfers free energy throughout the system temporarily storing it in different reservoirs such as the spin states of the bodies at different times. If too much energy is stored in certain kinetic energy reservoirs, the system can be irreversibly changed. These two reservoirs are: the spin energy of the secondary and the relative translational energy of the bodies. If too much energy is stored in the translational energy the system will disrupt, and if too much

energy is stored in the spin of the secondary then the secondary will fission. In other words, the secondary of the proto-binary can be rotationally accelerated via gravitational torques from the primary until it fissions, creating a chaotic ternary system. One or both secondaries may escape if the system has a positive free energy. Before escaping the secondaries may undergo further secondary fission event(s), creating a more complex system with three or more secondaries.

An alternative hypothesis for asteroid cluster formation mechanism was proposed by Vokrouhlický et al. (2017). They suggested that a swarm of small fragments could be formed by a cratering event, rather than a catastrophic disruption, from impact of a small projectile onto a nearly critically rotating primary. That might apply mainly to clusters where the population of secondaries is too numerous to be easily explained by the secondary fission process. Note for instance that Vokrouhlický et al. (2017) estimated that there are ~ 300 secondary fragments with size > 200 m in the Datura family. We assume that in such cases the initial trigger of the family formation was a collision. However, in contrast to the classical, collisionally-born asteroid families, the case of small asteroid families having parent bodies with $D < 20$ km offers a modified route. An impact of a small projectile onto a small parent body may cause a cratering or a fragmentation of the parent body. A fast rotation of the parent body may facilitate and boost the process, i.e., even a small impact may lead to escape of a number of fragments from the near-critically rotating parent body. Such cratering mechanism may result in a configuration similar to the outcome of the rotational fission process, evidenced by our data, only more simply explaining the multitude of small fragments found in some clusters.

An intriguing constraint on theories of asteroid cluster formation is placed by the properties of the Datura cluster discussed in Vokrouhlický et al. (2017). They found that the largest secondaries of the Datura cluster tend to have very elongated shapes (possibly contact binaries) and they tend to rotate relatively slowly. [13] Our observations of 10 secondaries of other asteroid clusters (see Section 3) showed, however, that only the largest secondary of the Schulhof cluster, (81337) 2000 GP36 had a high lightcurve amplitude indicating an elongated shape. The other 9 secondaries of the clusters of Irvine, Kap'bos, Hobson, (20674), Mandragora, Iochroma and Nicandra showed low to moderate lightcurve amplitudes < 0.7 mag. In Fig. 15, we plot the lightcurve amplitudes of secondaries of asteroid binaries (data from Pravec et al. 2016), [14] pairs (data by Pravec et al., in preparation) and clusters (data from Vokrouh-

[13] It is notable that all the observed cluster secondaries, of the Datura as well as the other clusters, appear to be in or close to principal axis rotation states. As their estimated excited rotation damping timescales are much longer than the age of the cluster (see Vokrouhlický et al. 2017), they were probably in or close to principal axis rotation when they escaped from the primary. This observation places another constraint on the cluster formation theories.

[14] The amplitudes of orbiting secondaries of asteroid binaries were calculated from the a_2/b_2 values given in Table 1 and Section 4.2 of Pravec et al. (2016) as $\mathcal{A}_2 = 2.5 \log(a_2/b_2)$, which gives an estimate for the opposition lightcurve amplitude.

lický et al. 2017 and this work). Except for the secondaries of the Datura and Schulhof clusters, the distribution of the secondary amplitudes (elongations) of the other 7 clusters agrees with the distributions for binaries and pairs, which are also thought to be formed by rotational fission. A reason for why just the Datura and Schulhof clusters contain very elongated secondaries remains to be found from future studies.

The tendency to relatively slow secondary rotations appears to be a common feature of all the clusters whose secondaries we observed. In Fig. 16, we show the distribution of secondary spin frequencies. The secondaries appear to have about a uniform distribution between $f = 0$ and 4 d^{-1} ($P > 6$ h), and they all are $f < 6$ d^{-1} ($P > 4$ h).[15] This is in marked contrast to the distribution of spin rates of the general asteroid population (with sizes comparable to the cluster members) by Pravec et al. (2008) who found the uniform distribution of asteroid spin rates between $f = 1$ and 9 d^{-1} and an excess of slow rotators with $f < 1$ d^{-1}. Among asteroid cluster secondaries, there are missing fast rotators with periods shorter than 4 hours[16] and there also does not appear to be present the excess of slow rotators (though this may be due to the low number statistics). A possible way for escaping secondaries to have a reduced spin rate can be related to gravitational torques during the escape process (Scheeres et al. 2000), or loss of secondary spin energy could also play a role in boosting the orbital energy of the secondary, similar to the loss of spin energy from the primary in rotational fission (Jacobson and Scheeres 2011).

Acknowledgements

We thank to Andrea Milani and an anonymous referee for their constructive criticism and useful comments that led us to improve the paper. The work at Ondřejov and observations with the Danish 1.54-m telescope on the ESO La Silla station were supported by the Grant Agency of the Czech Republic, Grants P209/12/0229 and 17-00774S. Computational resources for the orbital integrations were provided by the CESNET LM2015042 and the CERIT Scientific Cloud LM2015085, provided under the programme "Projects of Large Research, Development, and Innovations Infrastructures". Operations at Sugarloaf Mountain were supported by a Gene Shoemaker NEO grant from the Planetary Society. The work at Tatranská Lomnica was supported by the Slovak Grant Agency for Science VEGA, Grant 2/0032/14 and project ITMS No. 26220120009, based on the supporting operational Research and development program financed from the European Regional Development Fund. The work at Abastumani was supported by the Shota Rustaveli National Science Foundation, Grant FR/379/6-300/14. The work at Modra was supported by the Slovak Grant Agency for Science VEGA, Grant 1/0911/17. We thank

[15] We note that the two highest secondary spin rates —the two rightmost bins in Fig. 16— of the Datura cluster secondaries (215619) 2003 SQ168 and 2002 RH291 were somewhat poorly determined and they might be actually lower; see Vokrouhlický et al. (2017).

[16] Unlike among asteroid cluster secondaries, fast rotators with periods betwen 2 and 4 hours are frequent among asteroid pair secondaries (Pravec et al., in preparation).

B. Hafizov and O. Parmonov for their assistance during the observations at Maidanak in 2010.

References

Espy, A. J., et al., 2009. Evidence from IRAS for a very young, partially formed dust band. Planet. Space Sci. 57, 235-242.

Espy Kehoe, A. J., et al., 2015. Signatures of recent asteroid disruptions in the formation and evolution of Solar System dust bands. Astrophys. J. 811, 66.

Farnocchia, D. et al., 2013. Near Earth Asteroids with measurable Yarkovsky effect. Icarus 224, 1–13.

Guibout, V., Scheeres, D. J., 2003. Stability of Surface Motion on a Rotating Ellipsoid. Celest. Mech. Dyn. Astr. 87, 263–290.

Jacobson, S. A., Scheeres, D. J., 2011. Dynamics of rotationally fissioned asteroids: Source of observed small asteroid systems. Icarus 214, 161–178.

Knežević, Z., Milani, A., 2003. Proper element catalogs and asteroid families. Astron. Astrophys. 403, 1165–1173.

Knežević, Z., Lemaitre, A., Milani, A., 2002. The determination of asteroid proper elements. In Asteroids III, ed. W. F. Bottke et al. (Tucson: University of Arizona Press), 603–612.

Levison, H. F., Duncan, M. J., 1994. The long-term dynamical behavior of short-period comets. Icarus 108, 18–36.

Masiero, J. R. et al., 2011. Main belt asteroids with WISE/NEOWISE. I. Preliminary albedos and diameters. Astrophys. J. 741, 68–89.

Milani, A., Groncchi, G. F., 2010. Theory of orbit determination. Cambridge University Press, Cambridge.

Nesvorný, D., Bottke, W.F., Dones, L., Levison, H.F., 2002. The recent breakup of an asteroid in the main-belt region. Nature 417, 720–722.

Nesvorný, D., Vokrouhlický, D., 2006. New candidates for recent asteroid breakups. Astron. J. 132, 1950–1958.

Nesvorný, D., Vokrouhlický, D., Bottke, W.F., 2006. The breakup of a main-belt asteroid 450 thousand years ago. Science 312, 1490.

Nesvorný, D. et al., 2008. Origin of the near-ecliptic circumsolar dust band. Astrophys. J. 679, L143–L146.

Nesvorný, D., Carruba, V., Brož, M., 2015. Identification and dynamical properties of asteroid families. In: Asteroids IV (eds. P. Michel et al.), University

of Arizona Press, Tucson, 297–321.

Novaković, B. et al. 2014. Discovery of a young asteroid cluster associated with P/2012 F5 (Gibbs). Icarus 231, 300–309.

Pravec, P., Harris, A. W., 2007. Binary asteroid population. 1. Angular momentum content. Icarus 190, 250–259.

Pravec, P., Vokrouhlický, D., 2009. Significance analysis of asteroid pairs. Icarus 204, 580–588.

Pravec, P. et al. 2008. Spin rate distribution of small asteroids. Icarus 197, 497–504.

Pravec, P. et al. 2010. Formation of asteroid pairs by rotational fission. Nature 466, 1085–1088.

Pravec, P. et al. 2012. Absolute magnitudes of asteroids and a revision of asteroid albedo estimates from WISE thermal observations. Icarus 221, 365–387.

Pravec, P. et al. 2016. Binary asteroid population. 3. Secondary rotations and elongations. Icarus 267, 267–295.

Rosaev, A., Plávalová, E., 2017. On the young family of 18777 Hobson. Icarus 282, 326–332.

Rożek, A., Breiter, S., Jopek, T.J., 2011. Orbital similarity functions – application to asteroid pairs. Mon. Not. R. Astron. Soc. 412, 987-994.

Scheeres, D. J., 2002. Stability in the Full Two Body Problem. Celest. Mech. Dyn. Astron. 83, 155–169.

Scheeres, D. J., 2007. Rotational fission of contact binary asteroids. Icarus 189, 370–385.

Scheeres, D. J., 2009. Minimum energy asteroid reconfigurations and catastrophic disruptions. Planetary and Space Science 57, 154–164.

Scheeres, D. J., 2016. Hill Stability of Configurations in the Full N-Body Problem. In *Asteroids: New observations, New models*, Proc. of the Internat. Astron. Union S318, 128–134.

Scheeres, D. J., 2017. Relative Equilibria in the Full N-Body Problem with Applications to the Equal Mass Problem. In *Recent Advances in Celestial and Space Mechanics* (M. Chyba and B. Bonnard, eds.), Mathematics for Industry Vol. 23, Springer. ISBN 978-3-319-27462-1.

Scheeres, D. J., Ostro, S. J., Asphaug, E., Hudson, R. S., Werner, R. A., 2000. Effects of Gravitational Interactions on Asteroid Spin States. Icarus 147, 106-118.

Vereš, P. et al., 2015. Absolute magnitudes and slope parameters for 250,000 asteroids observed by Pan-STARRS PS1 Preliminary results. Icarus 261, 34–47.

Vokrouhlický, D., 1999. A complete linear model for the Yarkovsky thermal force on spherical asteroid fragments. Astron. Astrophys. 344, 362–366.

Vokrouhlický, D., Nesvorný, D., 2011. Half-brothers in the Schulhof family? Astron. J. 142:26 (8pp).

Vokrouhlický, D., Nesvorný, D., Bottke, W. F., 2008. Evolution of dust trails into bands. Astrophys. J. 672, 696–712.

Vokrouhlický, D. et al., 2009. Datura family: the 2009 update. Astron. Astrophys. 507, 495–504.

Vokrouhlický, D. et al., 2016. The Schulhof family: Solving the age puzzle. Astron. J. 151:56 (12pp).

Vokrouhlický, D. et al., 2017. The young Datura asteroid family: Spins, shapes and population estimate. Astron. Astrophys. 598, A91 (19pp).

Zappalà, V., Cellino, A., Farinella, P., Knežević, Z., 1990. Asteroid families. I. Identification by hierarchical clustering and reliability assessment. Astron. J. 100, 2030–2046.

Žižka, J. et al., 2016. Asteroids 87887-415992: The youngest known asteroid pair? Astron. Astrophys. 595, A20 (11pp).

Table 1: Cluster members, absolute magnitudes, distances from the primary and estimated ages. For the clusters of (1270) Datura and (2384) Schulhof see Vokrouhlický et al. (2016, 2017) and Sections 2 and 3.

Asteroid	H	$d_{\rm mean}$ (m/s)	$T_{\rm sep}$ (kyr)
(6825) Irvine	14.07	0.00	
(143797) 2003 WA112	16.62	73.40	1372^{+296}_{-120}
(180233) 2003 UU192	16.8	57.69	$2024^{(+393)}_{-536}$
(236156) 2005 UL291	17.5	87.16	1928^{+367}_{-73}
(10321) Rampo	14.60	0.00	
(294272) 2007 UM101	17.5	6.38	660^{+532}_{-178}
(451686) 2013 BR67	17.7	88.77	1378^{+925}_{-415}
2015 HT91	17.9	95.71	1151^{+1100}_{-441}
2016 TE87	18.1	46.90	852^{+464}_{-278}
2006 UA169	18.2	52.63	1665^{+718}_{-691}
2014 HS9	18.5	53.28	1239^{+629}_{-515}
(11842) Kap'bos	14.42	0.00	
(228747) 2002 VH3	17.16	1.15	409^{+570}_{-248}
(436415) 2011 AW46	18.2	0.49	see text
(14627) Emilkowalski	13.61	0.00	
(126761) 2002 DW10	15.3	22.26	1384^{+572}_{-346}
(256124) 2006 UK337	15.9	16.34	312^{+877}_{-86}
(224559) 2005 WU178	16.6	10.45	339^{+2544}_{-110}
(434002) 2000 SM320	16.9	120.33	2258^{+462}_{-366}
2014 UV143	17.4	103.76	3100^{+765}_{-805}
2009 VF107*	17.6		
(476673) 2008 TN44	17.7	117.96	3447^{+524}_{-898}
(16598) Brugmansia	14.69	0.00	
(190603) 2000 UV80	16.7	6.77	182^{+63}_{-64}
(218697) 2005 TT99	17.1	3.56	167^{+63}_{-47}
(18777) Hobson	15.16	0.00	
(57738) 2001 UZ160	15.41	4.24	405^{+367}_{-129}

Table 1: *cont.*

Asteroid	H	d_{mean} (m/s)	T_{sep} (kyr)
(436620) 2011 LF12	17.0	7.16	348^{+287}_{-144}
(363118) 2001 NH14	17.4	27.36	372^{+279}_{-86}
(465404) 2008 HQ46	17.5	38.65	321^{+222}_{-83}
(450571) 2006 JH35	17.6	31.83	318^{+87}_{-46}
(381414) 2008 JK37	17.7	10.65	384^{+269}_{-78}
2014 JJ10	17.8	27.38	310^{+350}_{-67}
2014 HH103	18.0	10.84	316^{+612}_{-81}
2015 KA91*	18.1		
2014 OJ66*	18.6		
(20674) 1999 VT1	12.81	0.	
(140429) 2001 TQ96	15.19	306.	2994^{+699}_{-516}
(341222) 2007 RT138	15.7	336.	1665^{+201}_{-122}
(257134) 2008 GY132	15.8	452.	1560^{+79}_{-117}
(177075) 2003 FR36	15.88	421.	1621^{+107}_{-122}
(249738) 2000 SB159	15.96	315.	1781^{+275}_{-210}
(321490) 2009 SH54	16.0	445.	1499^{+141}_{-60}
(389622) 2011 HU90	16.8	354.	1555^{+207}_{-219}
2002 TF325	17.1	469.	1808^{+819}_{-1292}
P/2012 F5	17.4		
(21509) Lucascavin	15.15	0.00	
(180255) 2003 VM9	16.8	7.40	367^{+640}_{-104}
(209570) 2004 XL40	17.1	4.82	881^{+270}_{-375}
(22280) Mandragora	14.02	0.00	
(324154) 2005 YN176	16.4	14.70	211^{+437}_{-114}
(180105) 2003 FB12	16.5	102.15	254^{+370}_{-82}
(284995) 2010 KF124	16.5	128.57	199^{+125}_{-41}
(472944) 2015 GH28	16.6	81.82	607^{+356}_{-418}
(296045) 2009 AX18	16.7	134.00	279^{+241}_{-77}
(446436) 2014 JY39	16.7	160.79	199^{+172}_{-43}
2013 EC88	16.7	107.55	206^{+503}_{-88}

Table 1: *cont.*

Asteroid	H	d_{mean} (m/s)	T_{sep} (kyr)
(459310) 2012 GZ32	16.9	13.02	355^{+395}_{-197}
2007 BJ41	17.2	34.65	442^{+460}_{-195}
(43239) 2000 AK238	14.90	710.06	316^{+31}_{-34}
(204960) 4713 P-L	16.2	2093.71	278^{+17}_{-11}
(265395) 2004 TM4	16.4	2103.52	283^{+21}_{-18}
(391017) 2005 SX208	16.6	1437.68	358^{+146}_{-15}
(327558) 2006 CE52	16.7	322.19	153^{+57}_{-39}
(412122) 2013 GQ30	16.7	472.58	226^{+68}_{-48}
(373667) 2002 QX88	16.9	1135.03	306^{+61}_{-46}
2008 HP40	17.1	682.20	288^{+88}_{-55}
2010 RY26	18.1	2075.75	339^{+227}_{-71}
(39991) Iochroma	14.79	0.00	
(349730) 2008 YV80	17.4	2.20	154^{+98}_{-50}
(340225) 2006 BR54	18.20	6.37	225^{+257}_{-105}
(428243) 2006 YE19	18.2	1.80	134^{+182}_{-35}
2005 UU94	18.4	12.23	231^{+168}_{-118}
(66583) Nicandra	14.91	0.00	
(279777) 1999 TT144	16.46	36.96	867^{+171}_{-25}
2008 SO34*	17.8		
2012 TF228*	18.2		
2014 QV272	18.9	45.57	868^{+598}_{-271}

Asteroids denoted with a star are one-opposition only.

Table 2
Primary sizes, periods and total secondary-to-primary mass ratios

Cluster primary	D_1 (km)	H_1	$H_{\rm seceq}$	ΔH	q	P_1 (h)
(1270) Datura	8.2	12.65	15.45	$2.80^{+0.06}_{-0.6}$	0.021	3.36
(2384) Schulhof	11.6	12.13	14.64	$2.51^{+0.09}_{-0.6}$	0.031	3.29
(6825) Irvine	4.6	14.07	16.09	$2.02^{+0.18}_{-0.18}$	0.061	3.62
(10321) Rampo	3.8	14.60	16.61	$2.01^{+0.14}_{-0.6}$	0.062	5.23
(11842) Kap'bos	4	14.42	17.01	$2.59^{+0.07}_{-0.07}$	0.028	3.69
(14627) Emilkowalski	6.9	13.61	14.86	$1.25^{+0.15}_{-0.6}$	0.178	11.13
(16598) Brugmansia	5	14.69	16.37	$1.68^{+0.32}_{-0.32}$	0.098	3.93
(18777) Hobson	3	15.16	15.15	$-0.01^{+0.06}_{-0.6}$	1.014	10.23
(20674) 1999 VT1	12	12.81	14.35	$1.54^{+0.09}_{-0.09}$	0.119	6.31
(21509) Lucascavin	3	15.15	16.43	$1.28^{+0.18}_{-0.18}$	0.171	5.79
(22280) Mandragora	9.8	14.02	14.25	$0.23^{+0.08}_{-0.6}$	0.728	28.48
(39991) Iochroma	3	14.79	16.93	$2.14^{+0.20}_{-0.20}$	0.052	3.44
(66583) Nicandra	6.0	14.91	16.28	$1.37^{+0.17}_{-0.6}$	0.151	6.46

Note: The primary diameters given to 0.1 km have uncertainties about 10%, while those given to 1 km are more uncertain. Uncertainties of the mass ratios can be derived from the ΔH uncertainties using Eq. (5). Uncertainties for the primary absolute magnitudes and periods are given in Section 3 and Electronic Supplementary Information.

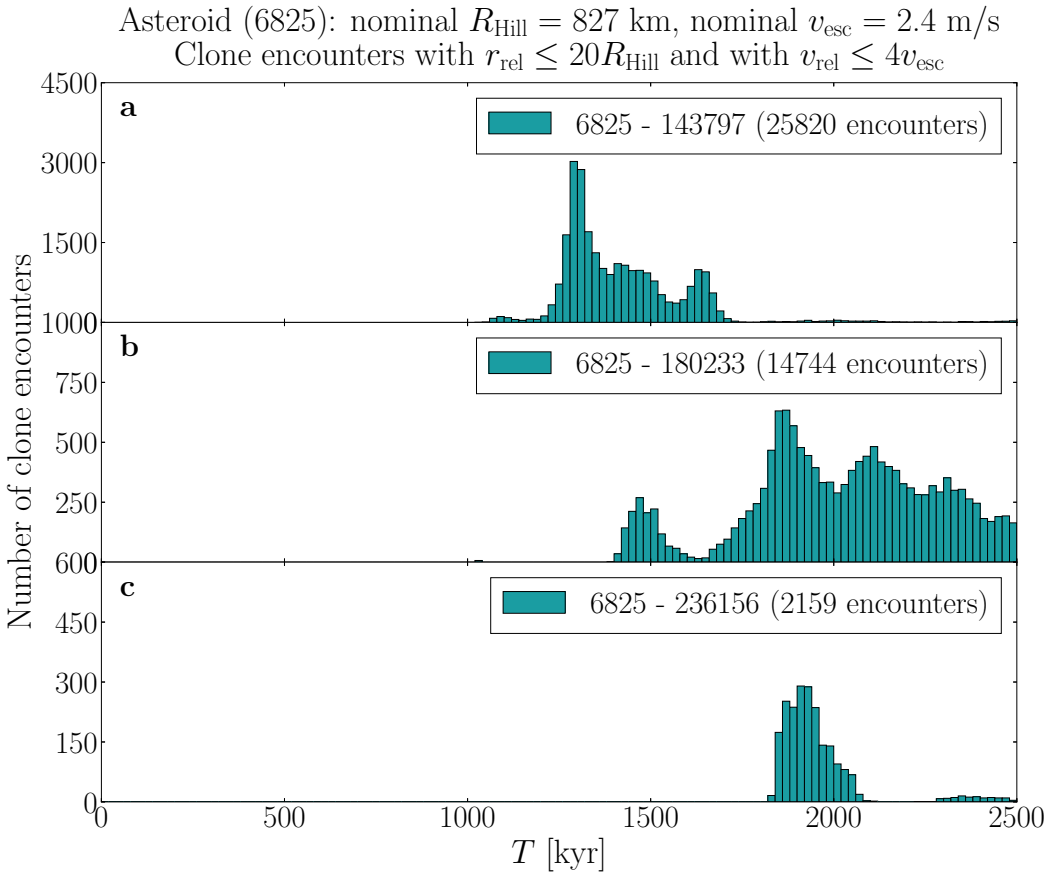

Fig. 1. Distribution of past times of close and slow primary–secondary clone encounters for the three secondaries (143797) 2003 WA112, (180233) 2003 UU192 and (236156) 2005 UL291 of the cluster of (6825) Irvine.

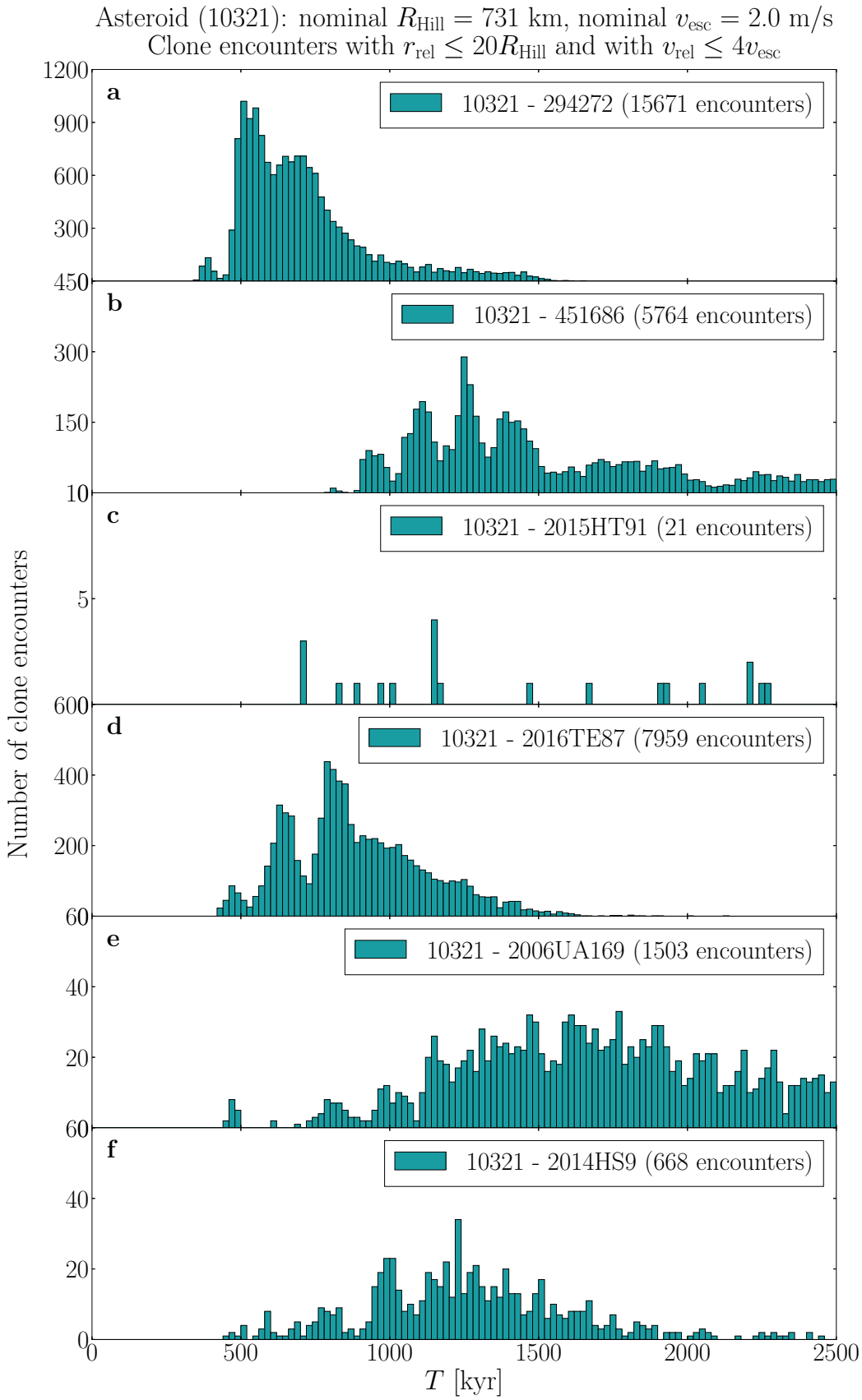

Fig. 2. Distribution of past times of close and slow primary–secondary clone encounters for the six secondaries (294272) 2007 UM101, (451686) 2013 BR67, 2015 HT91, 2016 TE87, 2006 UA169 and 2014 HS9 of the cluster of (10321) Rampo.

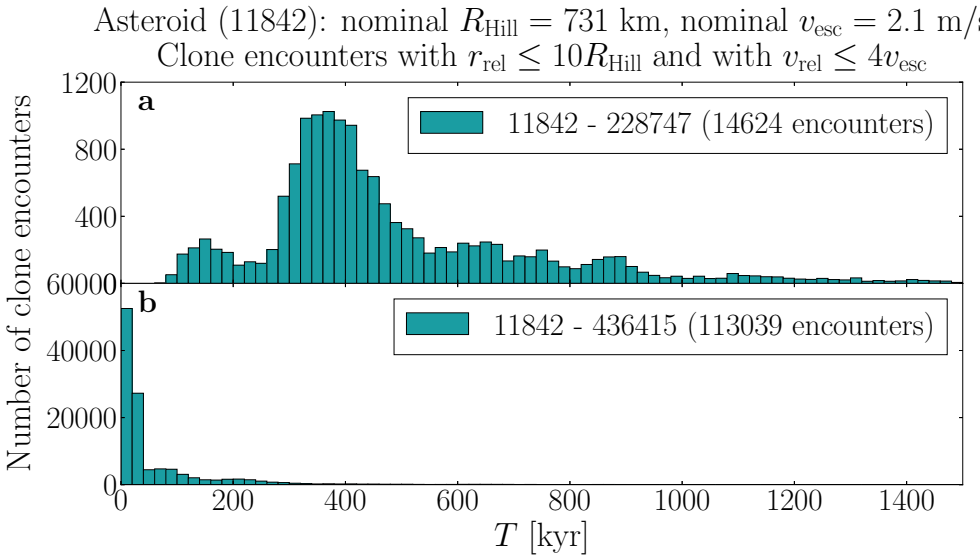

Fig. 3. Distribution of past times of close and slow primary–secondary clone encounters for the two secondaries (228747) 2002 VH3 and (436415) 2011 AW46 of the cluster of (11842) Kap'bos.

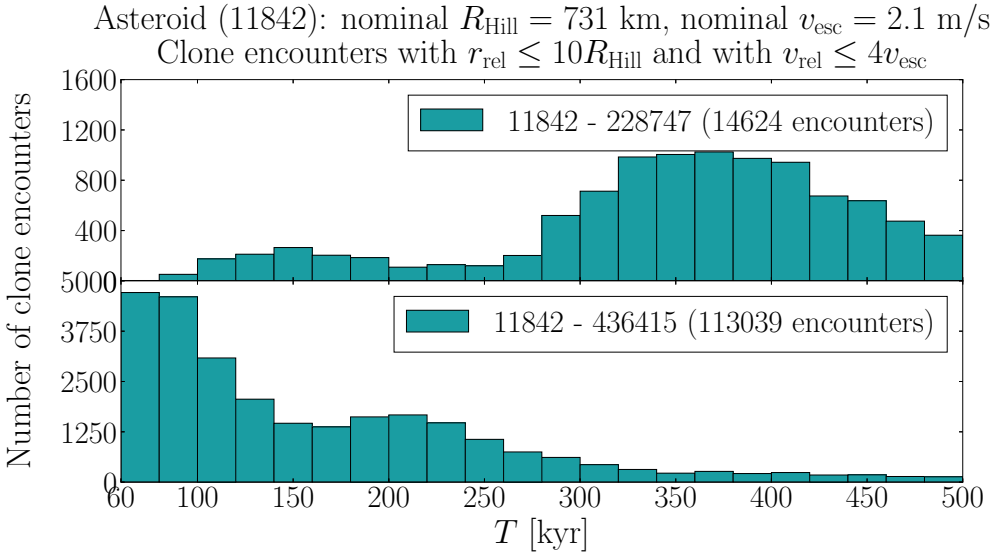

Fig. 4. A detail of the distribution of past times of close and slow primary–secondary clone encounters of the cluster of (11842) Kap'bos.

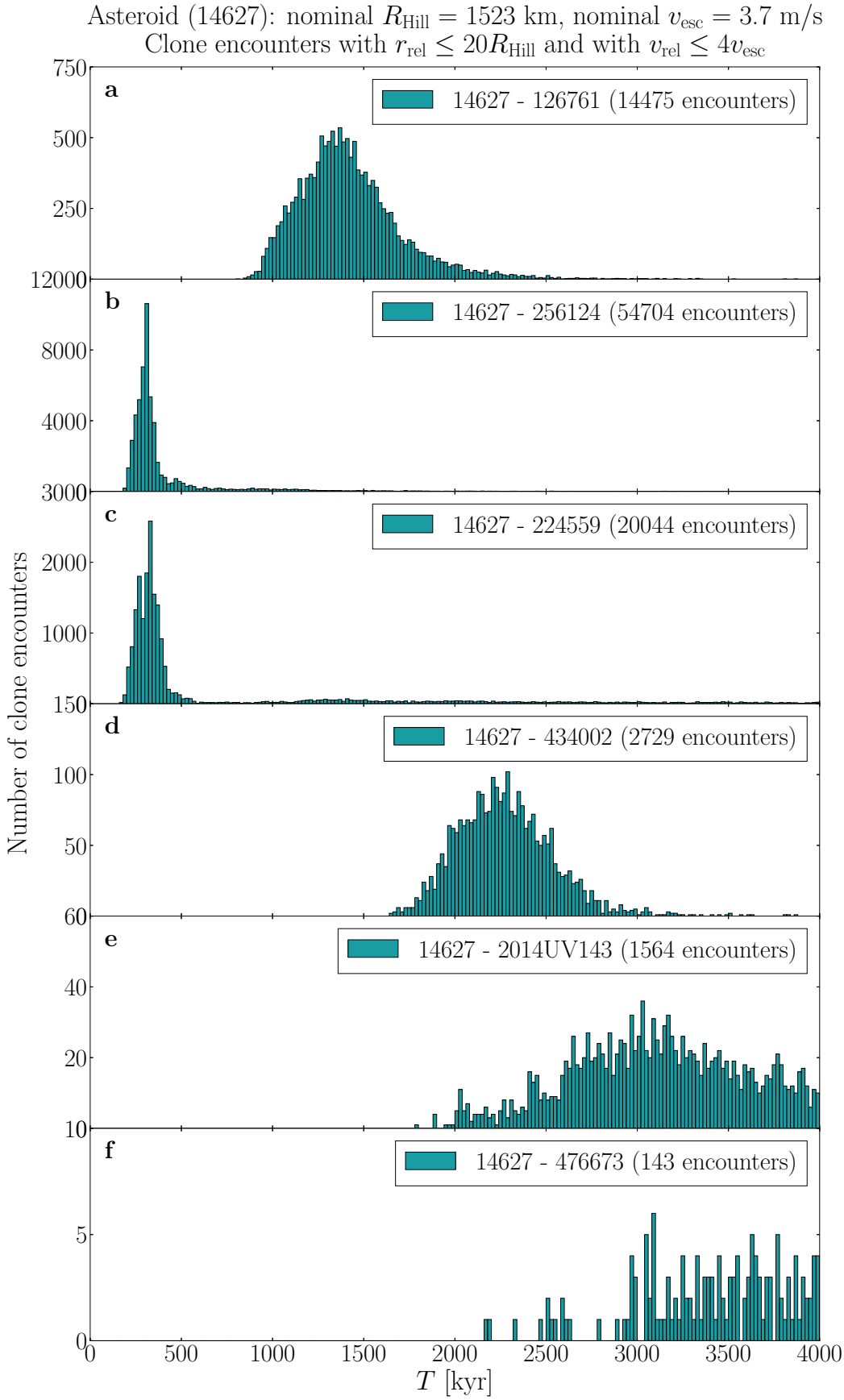

Fig. 5. Distribution of past times of close and slow primary–secondary clone encounters for the six secondaries (126761) 2002 DW10, (256124) 2006 UK337, (224559) 2005 WU178, (434002) 2000 SM320, 2014 UV143 and (476673) 2008 TN44 of the cluster of (14627) Emilkowalski.

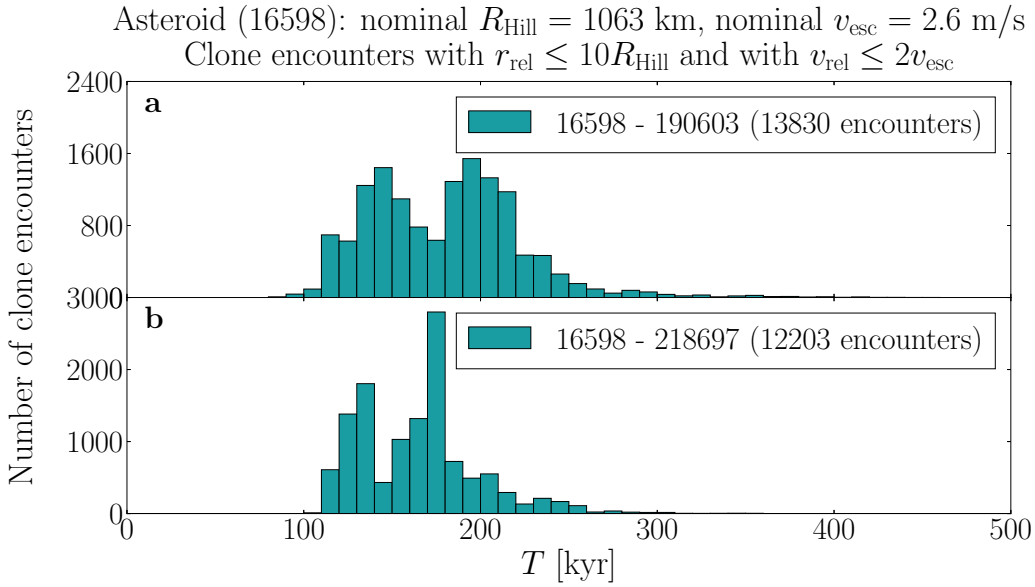

Fig. 6. Distribution of past times of close and slow primary–secondary clone encounters for the two secondaries (190603) 2000 UV80 and (218697) 2005 TT99 of the cluster of (16598) Brugmansia.

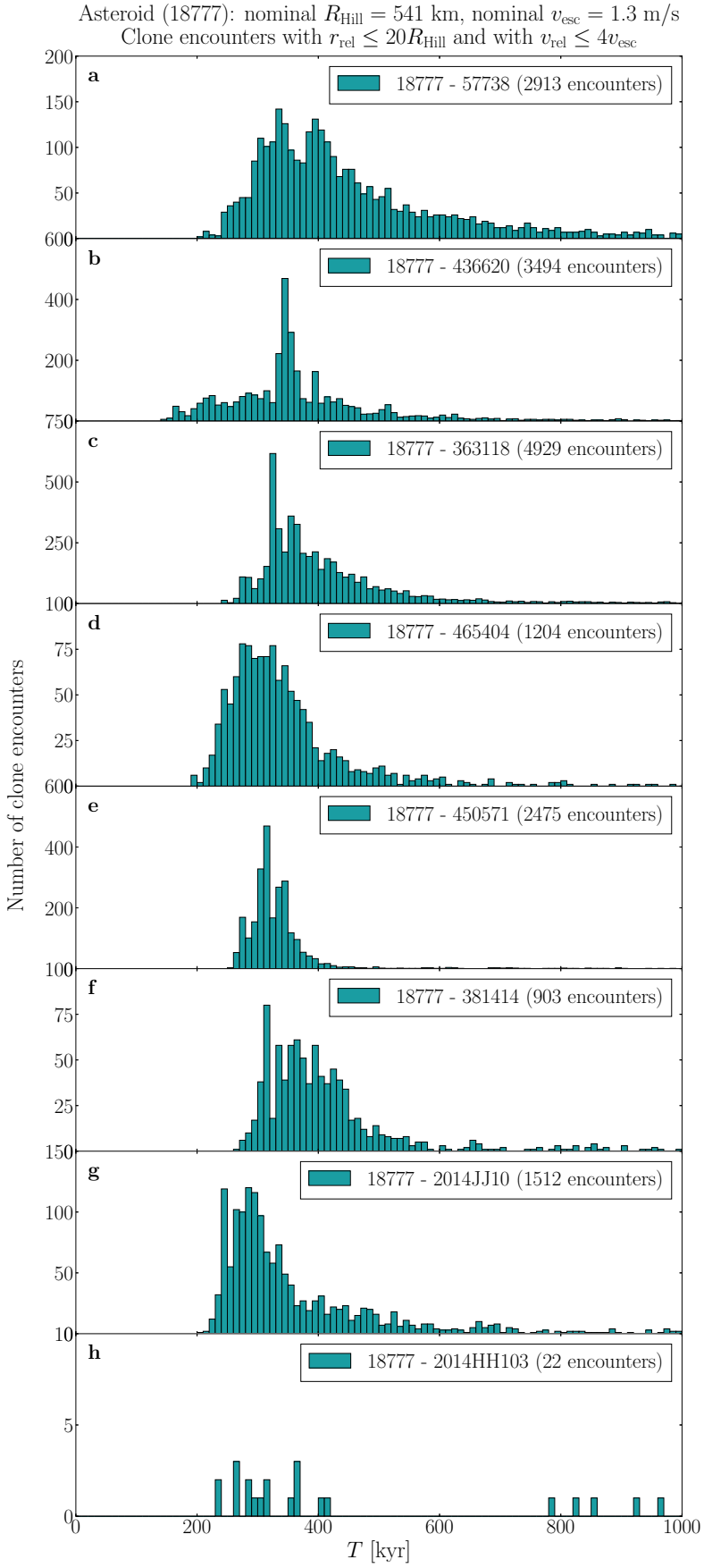

Fig. 7. Distribution of past times of close and slow primary–secondary clone encounters for the eight secondaries (57738) 2001 UZ160, (436620) 2011 LF12, (363118) 2001 NH14, (465404) 2008 HQ46, (450571) 2006 JH35, (381414) 2008 JK37, 2014 JJ10 and 2014 HH103 of the cluster of (18777) Hobson.

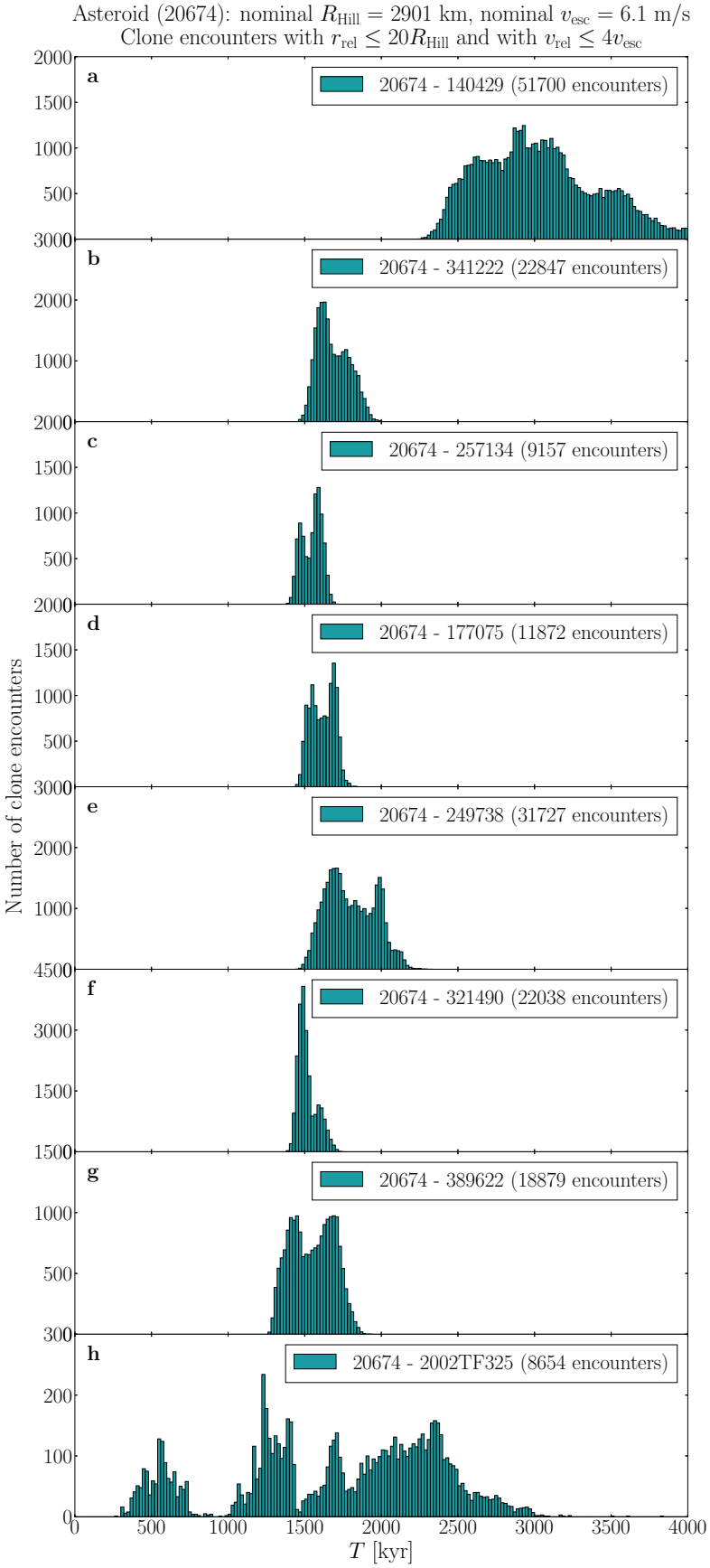

Fig. 8. Distribution of past times of close and slow primary–secondary clone encounters for the eight secondaries (140429) 2001 TQ96, (341222) 2007 RT138, (257134) 2008 GY132, (177075) 2003 FR36, (249738) 2000 SB159, (321490) 2009 SH54, (389622) 2011 HU90 and 2002 TF325 of the cluster of (20674) 1999 VT1.

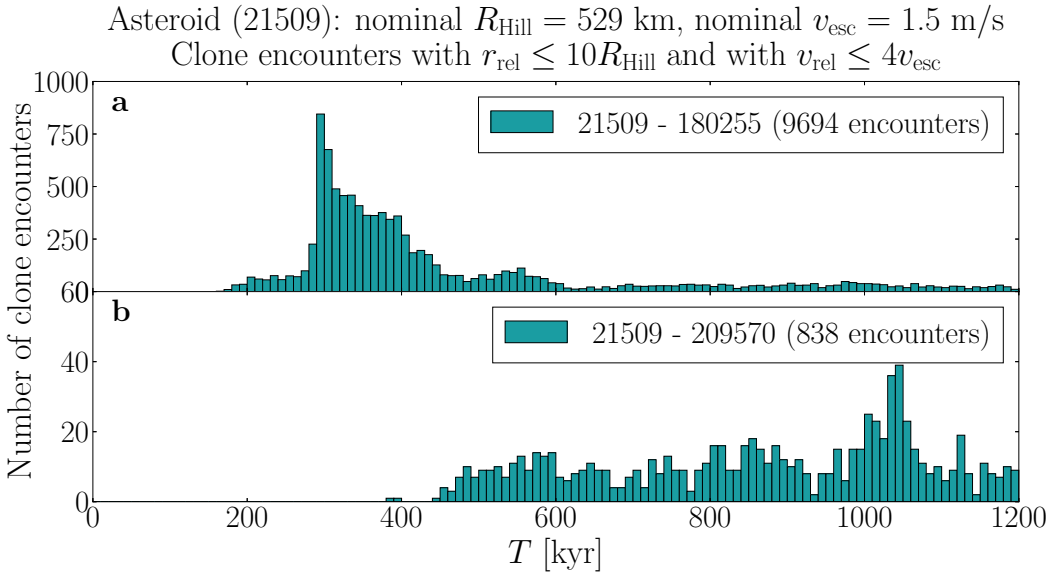

Fig. 9. Distribution of past times of close and slow primary–secondary clone encounters for the two secondaries (180255) 2003 VM9 and (209570) 2004 XL40 of the cluster of (21509) Lucascavin.

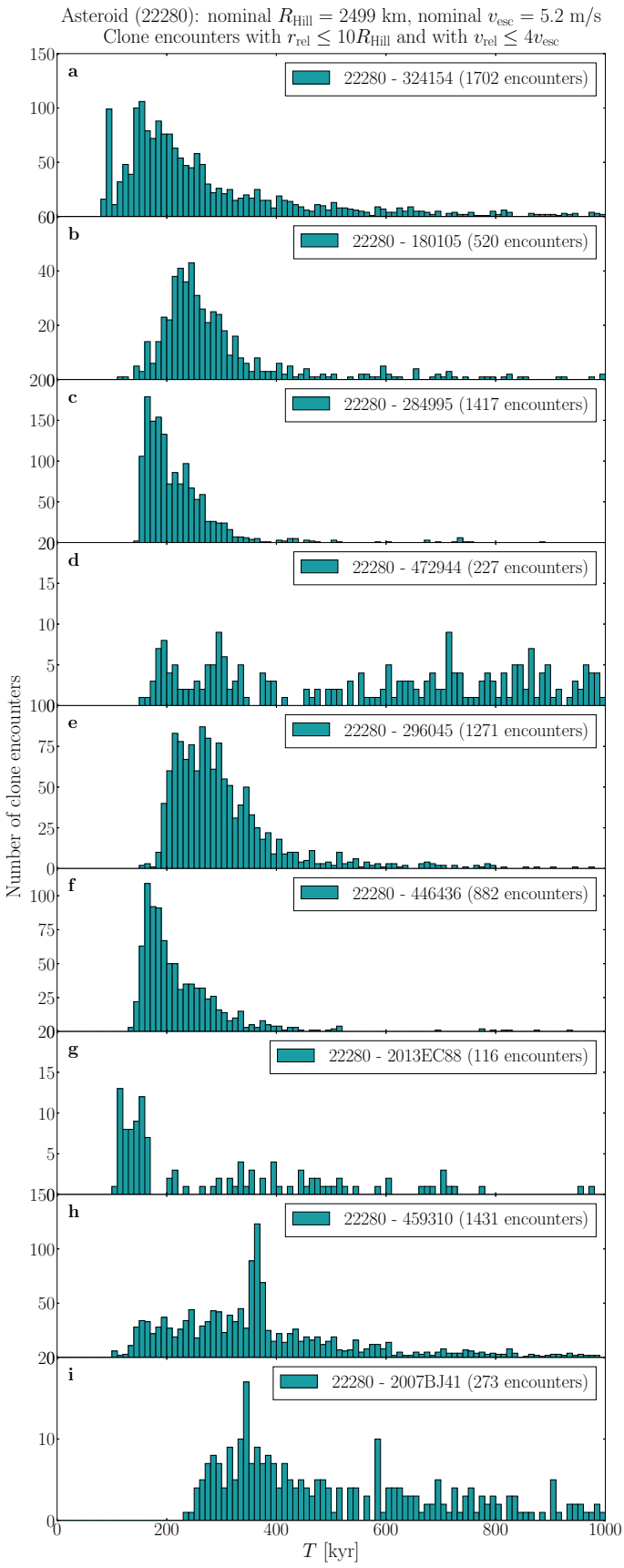

Fig. 10. Distribution of past times of close and slow primary–secondary clone encounters for the nine secondaries (324154) 2005 YN176, (180105) 2003 FB12, (284995) 2010 KF124, (472944) 2015 GH28, (296045) 2009 AX18, (446436) 2014 JY39, 2013 EC88, (459310) 2012 GZ32 and 2007 BJ41 (with $d_{\rm mean} < 161$ m/s) of the cluster of (22280) Mandragora.

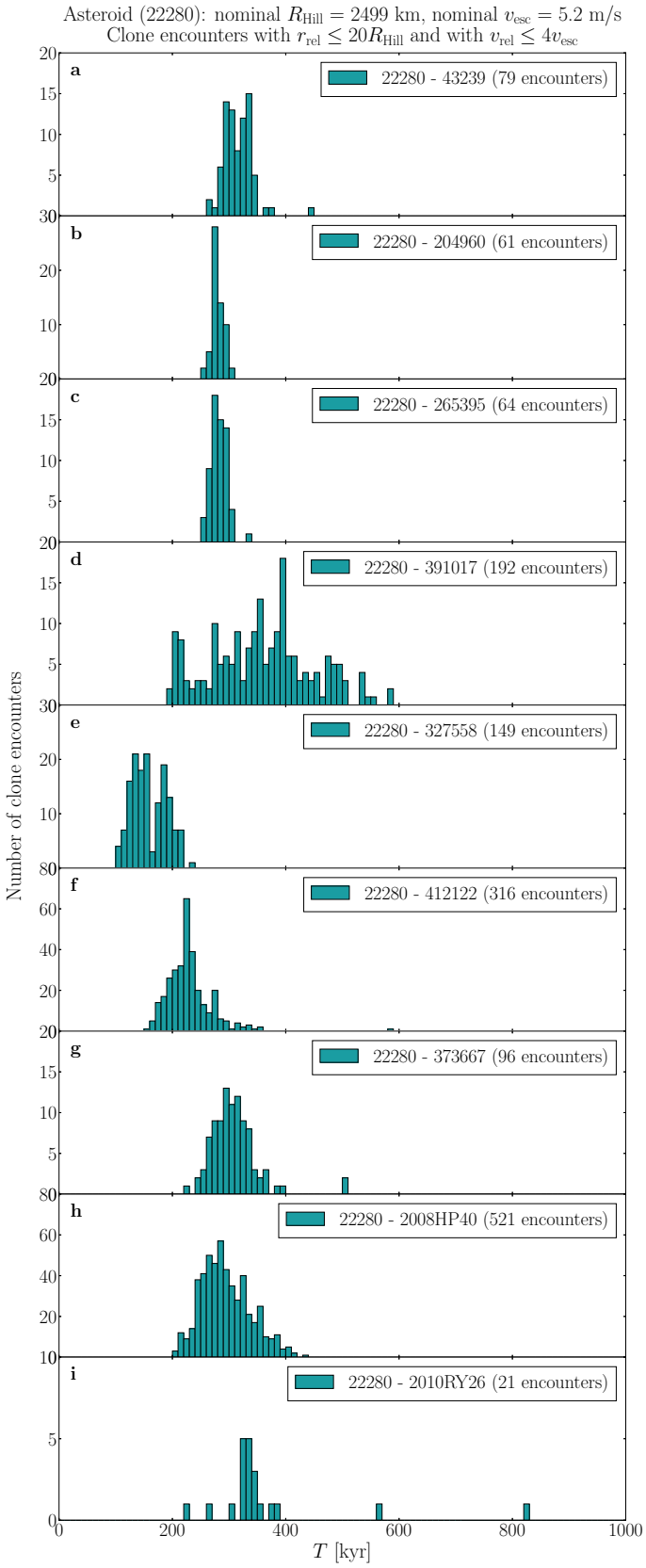

Fig. 11. Distribution of past times of close and slow primary–secondary clone encounters for the nine secondaries (43239) 2000 AK238, (204960) 4713 P-L, (265395) 2004 TM4, (391017) 2005 SX208, (327558) 2006 CE52, (412122) 2013 GQ30, (373667) 2002 QX88, 2008 HP40 and 2010 RY26 (with $d_{\rm mean} > 322$ m/s) of the cluster of (22280) Mandragora.

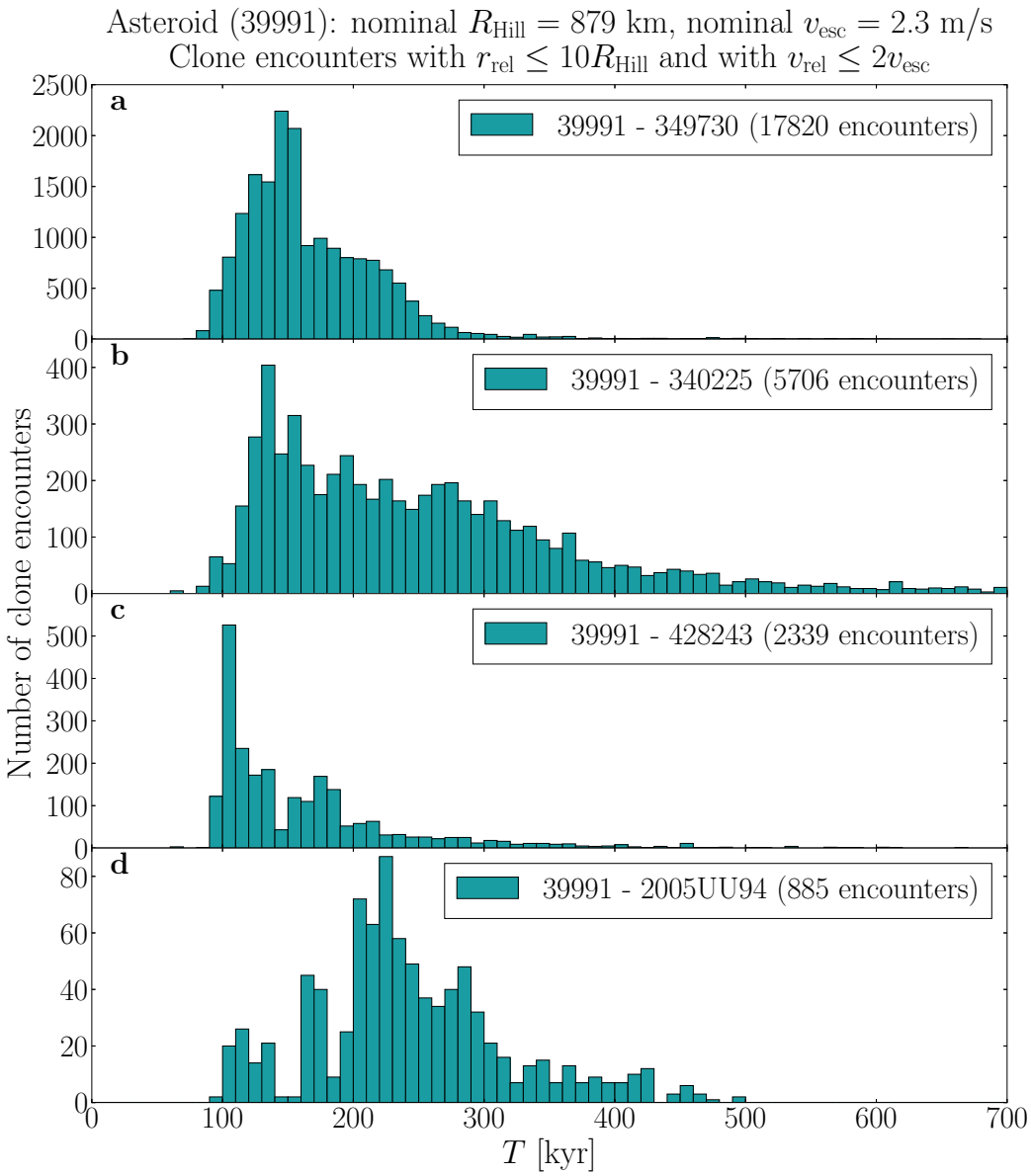

Fig. 12. Distribution of past times of close and slow primary–secondary clone encounters for the four secondaries (349730) 2008 YV80, (340225) 2006 BR54, (428243) 2006 YE19 and 2005 UU94 of the cluster of (39991) Iochroma.

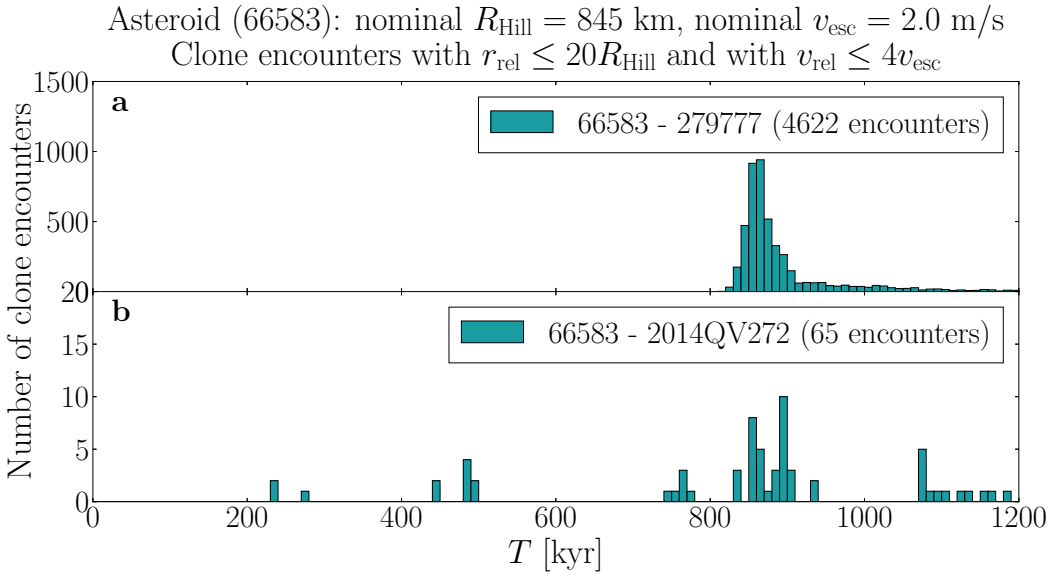

Fig. 13. Distribution of past times of close and slow primary–secondary clone encounters for the two secondaries (279777) 1999 TT144 and 2014 QV272 of the cluster of (66583) Nicandra.

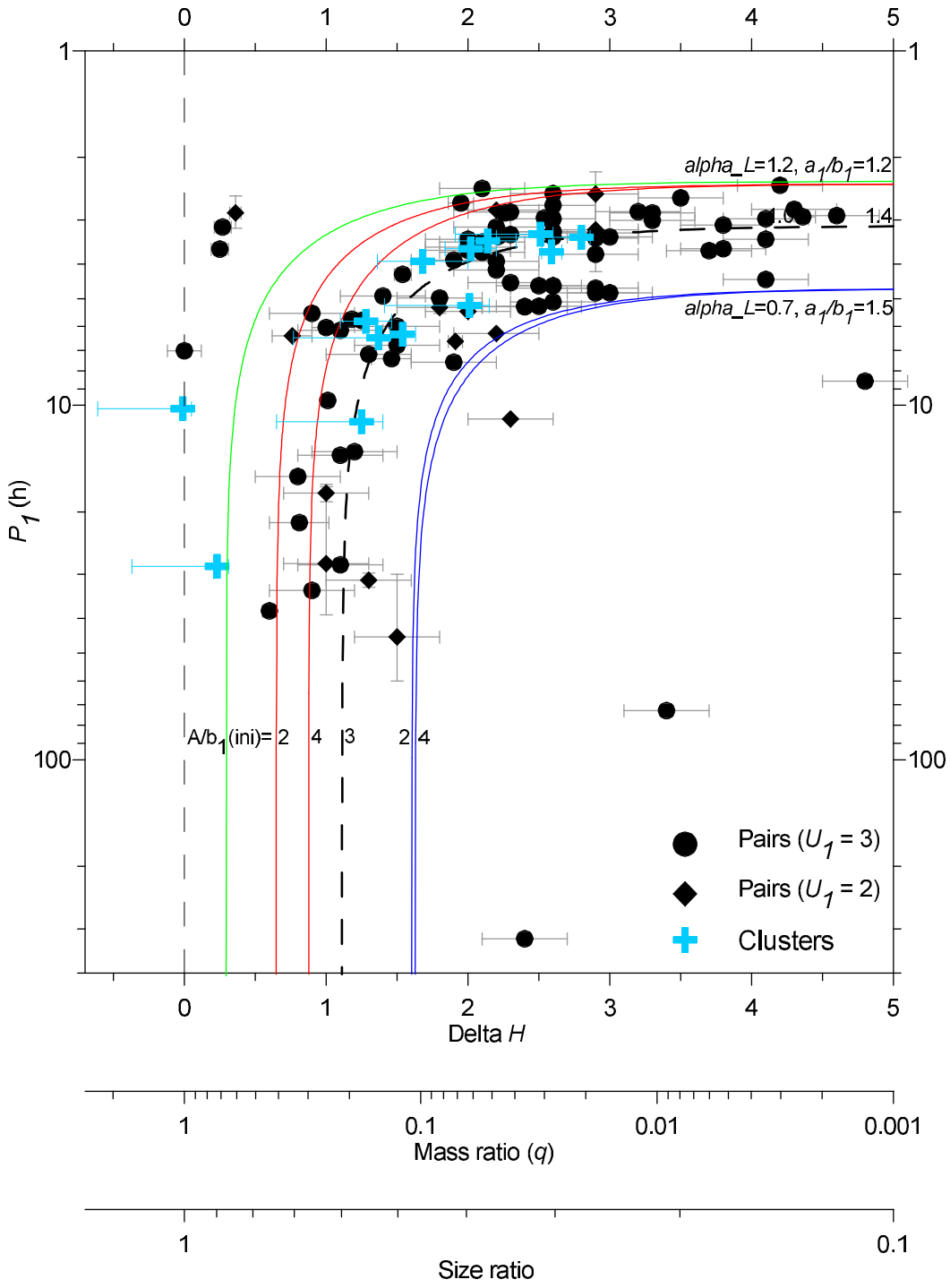

Fig. 14. Asteroid clusters mostly follow the same trend of primary period vs mass ratio as asteroid pairs, in agreement with the theory of their formation by rotational fission. The two exceptions are the high-mass ratio clusters of Hobson and Mandragora, see text. For description of the dashed black and continuous blue, red and green curves see the last paragraph of Section 5.

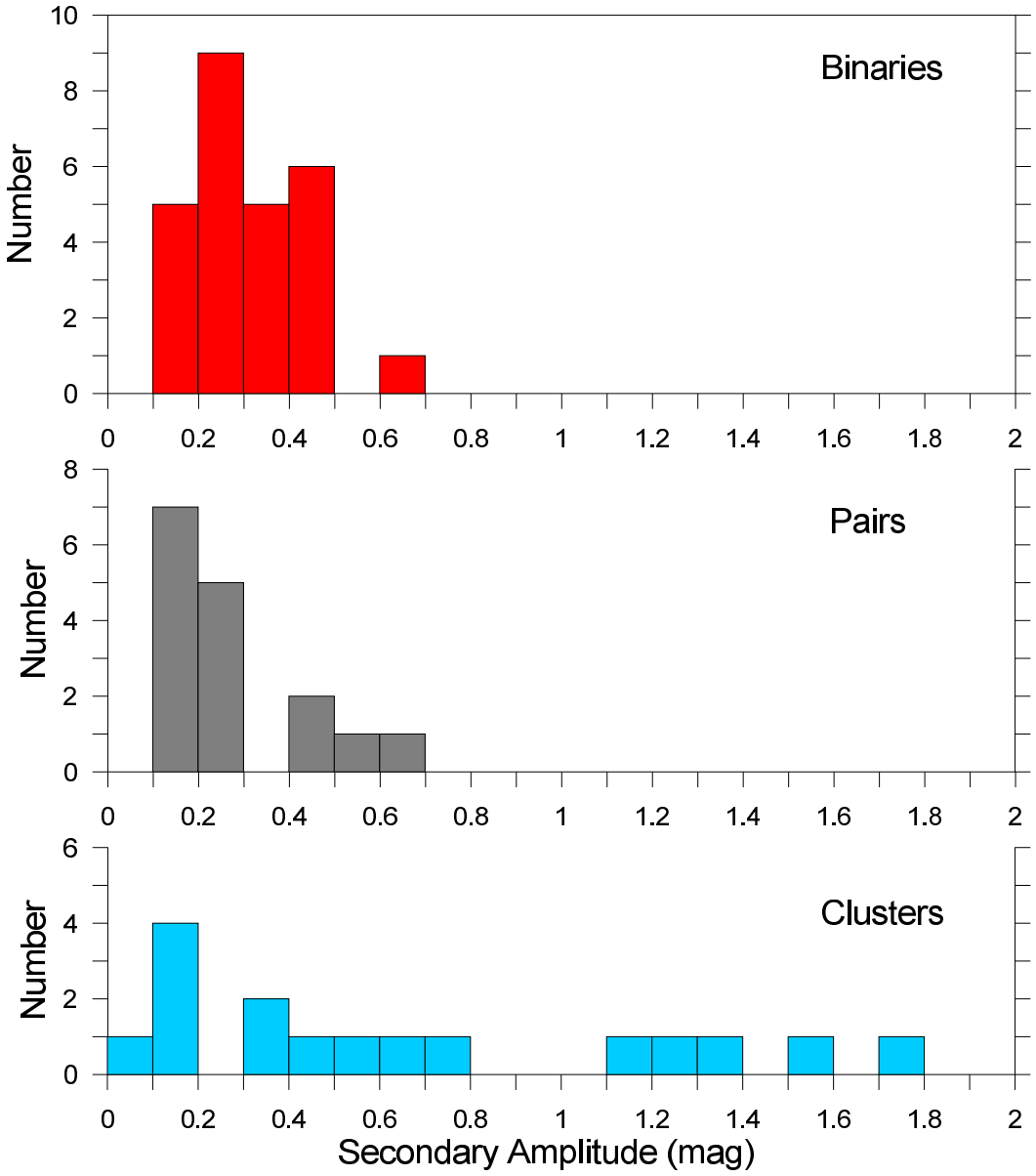

Fig. 15. Lightcurve amplitudes of secondaries of asteroid binaries (upper panel), pairs (middle panel) and clusters (lower panel). The tail of asteroid cluster secondaries to large amplitudes is due to the clusters of Datura and Schulhof, see text. Note: There is an observational bias against secondaries with low elongations in the asteroid binaries sample (see Pravec et al. 2016); amplitudes $\lesssim 0.2$ mag in orbiting secondaries are observationally demanding to reveal so they are underrepresented in our sample and the real number of binary secondaries in the two leftmost bins is probably higher than shown in the upper panel.

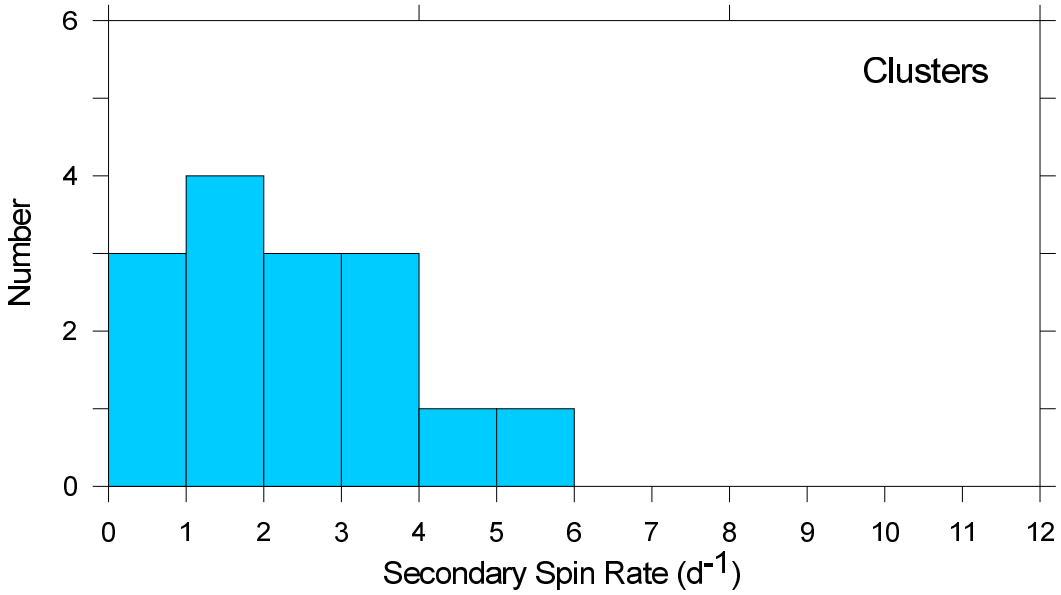

Fig. 16. Rotation frequencies of secondaries of asteroid clusters.